Operation of Inductive Charging Systems Under Misalignment Conditions: A Review for Electric Vehicles

Van-Binh Vu 🆔, *Member, IEEE*, Ali Ramezani 🆔, *Member, IEEE*, Alicia Triviño 🆔, *Member, IEEE*,
José M. González-González 🆔, Nasiru B. Kadandani 🆔, *Member, IEEE*,
Mohamed Dahidah 🆔, *Senior Member, IEEE*, Volker Pickert 🆔, *Member, IEEE*,
Mehdi Narimani 🆔, *Senior Member, IEEE*, and Jose Aguado 🆔, *Member, IEEE*

Abstract—Inductive power transfer (IPT) for electric vehicles (EVs) is an emerging technology that can transfer power wirelessly over certain distances, thus offering some remarkable characteristics in terms of flexibility, position, and movability. The output power of an IPT system depends on the coupling factor of the magnetic couplers, which can deviate from the nominal operating conditions due to the occurrence of misalignment. Nevertheless, misalignment of the magnetic couplers in inductive charging is inevitable, and it usually results in the variation of the mutual inductance and output power of the system with a corresponding decrease in the system's overall efficiency. So far, the literature has reported various techniques for achieving designs with higher misalignment tolerance. The reported techniques can be mainly classified into three categories, as viewed from the following aspects: magnetic couplers layouts, compensation networks, and control strategy. Each of these techniques has its pros and cons in terms of implementation cost, system layout, efficiency, power density, and reliability depending on the application. With the increased investigation of more applications of IPT, new modified techniques for improving the misalignment tolerance in the IPT system are continuously being proposed based on permutations and combinations of the existing ones; thus causing some confusion and difficulties for researchers and system vendors to follow. This article, therefore, aims to provide a comprehensive review of the existing methods for IPT systems that address the misalignment issue in EVs' wireless charging. The background of the inductive charging systems for EVs is presented and an investigation of the numerous factors affecting the output power and other performances is conducted. In addition, the advantages and disadvantages of each technique on the IPT system's performance are analyzed in detail.

Index Terms—Compensation circuits, control in wireless charging, electric vehicle (EV) wireless battery charging, magnetic couplers.

I. INTRODUCTION

THE progression and popularization of battery-powered devices are limited by some fundamental issues, such as the electricity storage technology due to its unsatisfactory energy density, limited lifetime, and high initial cost. Inductive power transfer (IPT) technology has been proposed to address the outstanding issues associated with energy storage while offering remarkable characteristics in terms of position and mobility. This developing technology has received much attention from both industry and academia. It allows the device battery to be charged frequently and without a manual connection, which results in a significant reduction of its battery size. The limits of energy storage technology in all kinds of battery-powered devices can be fundamentally tackled by applying the novel wireless charging technique. Applications of IPT technology can be classified into high- and low-power levels. The high-power level category includes power systems, manufacturing automation, and electric vehicles (EVs). On the other hand, the low-power level category refers to implanted medical devices, consumer electronics, integrated circuits, and so forth.

The inductive charging for EVs is made up of two separate parts referred to as the primary and secondary sides. Fundamentally, the primary side is equipped with a transmitter winding that is driven by a high-frequency alternating current (ac) current being controlled by an inverter and a primary resonant circuit. The inverter is powered by a dc voltage source, which is rectified from the mains. The high-frequency ac current generates the magnetic fields and powers the receiver coil, which is installed on the secondary side. The receiver coil is usually connected to a secondary resonant tank and a rectifier to convert the power from ac to direct current (dc). The rectifier is then connected to the output battery. The induced voltage on the secondary coil depends on the mutual inductance; thus, relative positions between the transmitter and the receiver play a crucial role in determining the overall system efficiency and

Van-Binh Vu is with Turbo Power Systems, Gateshead NE11 0QD, U.K., and also with the School of Engineering, Newcastle University, Newcastle upon Tyne NE1 7RU, U.K. (e-mail: binh.vu@ncl.ac.uk).

Ali Ramezani was with Department of Electrical and Computer Engineering, McMaster University, Hamilton, ON L8S 4L8, Canada. He is now with eLeapPower, Toronto, ON M3A 1A1, Canada (e-mail: aliramezani@ieee.org).

Alicia Triviño, José M. González-González, and Jose Aguado are with the Department of Electrical Engineering, University of Malaga, 29071 Málaga, Spain (e-mail: atc@uma.es; josemanuelgonzalez@uma.es; jaguado@uma.es).

Nasiru B. Kadandani, Mohamed Dahidah, and Volker Pickert are with the School of Engineering, Merz Court, Newcastle University, Newcastle upon Tyne NE1 7RU, U.K. (e-mail: nbkadandani.ele@buk.edu.ng; mohamed.dahidah@newcastle.ac.uk; volker.pickert@newcastle.ac.uk).

Mehdi Narimani is with the Department of Electrical and Computer Engineering, McMaster University, Hamilton, ON L8S 4L8, Canada (e-mail: narimanm@mcmaster.ca).
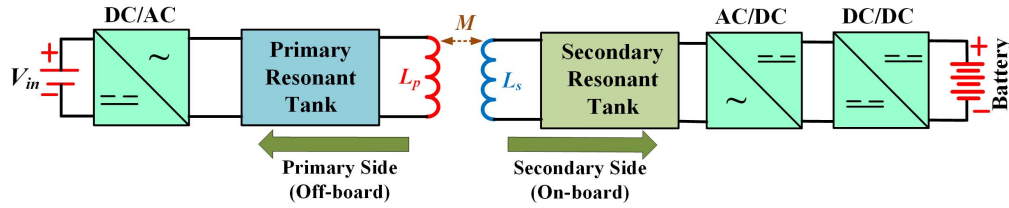
Fig. 1.   Functional structure of an EV wireless charger.

power transfer capability. Higher values of efficiency can only be achieved under perfect alignment conditions between the couplers. However, misalignment between the coils (vertical, horizontal, angular, or a combination of the previous ones) is inevitable in EVs' inductive charging, hindering room for achieving higher output power and efficiency. This provides a challenging motivation for the design and implementation of an IPT system with a view to addressing these challenges. In the light of this, numerous studies have been devoted to the techniques of improving the IPT system's performance under the coupler's misalignment conditions.

A review of the literature on IPT technology for EV applications revealed that the previous survey/review works were mainly focused on the following aspects.

1) Overall principle, current research topics, and future development trends of IPT technology, as reported in [1]–[3], where [1] and [2] extensively review the general background and fundamental technical issues. On the other side, more details on charging requirements and comparisons between the conductive and inductive charging methods are mentioned in [3].

2) IPT for transportation applications in general [4]–[8] and for EV's dynamic wireless charging in particular [9]–[11]. These references present the state-of-the-art review of the EVs' wireless charging, coupler coil topologies, compensation network, safety concerns, control methods, and relevant charging standards.

3) IPT for small air-gap (contactless) applications [12] or for mid-range air-gap applications [13]. These IPT systems normally have a smaller power rating and operate at a high operating frequency.

4) Compensation (resonant) circuit topologies for IPT systems [14], [15]. These studies review, analyze, and compare the main features of the compensation topologies, such as resonant characteristics, coupling coefficient dependent, output load-independent sources, effects on the soft-switching, and/or zero-phase-angle of the inverter.

5) Inductive pad (coils) topologies for IPT EVs stationary charging systems [16]. This study provides a comprehensive review of the structures of transmitter/receiver pads, and summarizes and compares various types of conductive winding materials, magnetic core materials, and pad shielding topologies.

6) New material for IPT charger systems, such as using metamaterials [17], [18]. These materials aim for a mid-range IPT approach where both efficiency and distance are extended. Metamaterials are artificially engineered materials that own different characteristics compared to electromagnetic ones. The two important features are evanescent wave amplification and negative refractive, which contributes, as key factors, to the improvement of the transfer efficiency [18].

7) Foreign object detection (FOD) and protection for the IPT charging [19]. It is well known that the metal objects surrounding the IPT charger will be heated up by the system's strong magnetic field. New development of IPT chargers will need to have different ways to detect the metals and protect the system under such scenarios.

However, to the best of our knowledge, there is no existing paper so far that reviews thoroughly the operation of an EVs inductive charging system under misalignment conditions. In the meanwhile, new techniques and configurations of IPT topologies are continuously being proposed to cater to the ever-increasing demand for various scenarios to operate in an arbitrary position. The lack of recompilation and explanation of these techniques and configurations may cause some confusions and difficulties for researchers and system vendors to follow. Therefore, this article reviews, compares, and evaluates different techniques of operating an inductive charging under misalignment conditions focusing more on EV battery charging applications.

II. EVs' WIRELESS CHARGER OPERATION

The functional structure of an EV wireless charger is illustrated in Fig. 1, in which V_{in} is the input dc voltage source and typically varies from 350 to 500 VDC according to the Society of Automotive Engineers (SAE) J2954 standard [20]. L_p is the self-inductance of the transmitter coil, L_s is the self-inductance of the receiver coil, and M is the mutual inductance between the transmitter and the receiver. V_{in} is normally generated using a front-end ac/dc converter (single-phase or three-phase depending on the power levels) and is usually equipped with the power factor correction (PFC) functionality. On the primary side, a dc/ac converter is used to convert V_{in} into a high-frequency ac voltage, which is fed to the primary compensation tank that consists of resonant inductors and capacitors. The primary resonant (compensation) tank compensates for the reactive power of the large leakage inductance of the magnetic coupler and acts as a low-pass filter that passes the fundamental-frequency signal and impedes

high-frequency signals. Therefore, the primary transmitter L_p is supplied by a sinusoidal ac current. The output power of the wireless system is directly proportional to the transmitter current [1]. However, to simplify the output power control strategy, the transmitter current is kept constant in many cases. Another resonant tank is placed on the secondary side to improve the system efficiency and the power transfer capability. It also cancels the high leakage inductance from the magnetic coupler unit. The induced voltage at the receiver coil after going through the resonant tank is rectified by an ac/dc converter, and a dc/dc converter is then used to regulate the charging current and voltage across the battery. Unlike the conductive charger, the primary side of the wireless charger is located off-board, while the secondary side is placed on the vehicle.

The major difference between a wireless charger and the conventional conductive charger is that the former is equipped with a set of loosely coupled coils (magnetic coupler), while the latter is based on a conventional transformer. A low coupling coefficient between the transmitter and receiver coils is one of the most challenging issues in an inductive wireless charging system. It usually results in high reactive power and reduces the power transfer efficiency of the system [1], [2], [4], [5]. Therefore, proper design and optimization of the magnetic coupler's parameters are essential in order to improve the coupling coefficient, extend the power transfer limit, and minimize the electromagnetic field exposed to pedestrians and passengers. As shown in Fig. 2(a), a magnetic coupler typically consists of winding, magnetic cores, and shielding. Each element of the magnetic coupler can be produced from different types and materials [16]. The windings can be made from different winding types, such as Litz, magnetoplate, magnetocoated, tubular copper, rare-earth barium copper oxide (REBCO), and copper–clad–aluminum (Cu-clad-Al) with different characteristics. Furthermore, magnetic cores play an important role in improving the coupling coefficient. The following materials are commonly used in an IPT system: ferrite, nanoparticle, magnetizable concrete, and flexible core. The magnetic core is normally created by stacking together from multiple blocks of magnetic bars. The shape of the magnetic core depends on the pad's structure and can be briefly classified into three following categories [1]: 1) plate-based shape [21]; 2) bar-based shape [22], [23]; and 3) tile-based shape [24]. Fig. 1(c) demonstrates the classification with the illustration diagrams for each core shape. To reduce the magnetic leakage fields, different types of shielding are utilized, such as passive, active, and reactive. Fig. 2(b) illustrates a simplified circuit model of the magnetic coupler. The relationship between the mutual inductance M, the self-inductance of the transmitter L_p, and the self-inductance of the receiver L_s is given by

$$k = \frac{M}{\sqrt{L_p L_s}} \tag{1}$$

where k is the coupling coefficient that indicates how strong the coupling between L_p and L_s is.

L_p is normally driven by the transmitter current, I_p, regardless of both mutual inductance and load resistance values.
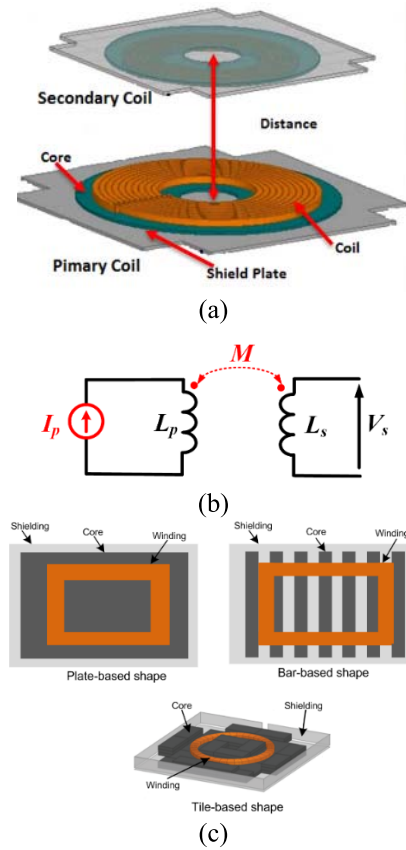

Fig. 2. (a) Typical structure of a magnetic coupler. (b) Simplified circuit model of the magnetic coupler. (c) Different shapes of the magnetic cores.

The transmitter current I_p is kept constant by controlling the primary inverter or by utilizing an LC circuit on the primary side. The induced voltage, V_s, on the receiver side can be expressed as

$$V_s = j\omega M I_p \tag{2}$$

where $\omega = 2\pi f$ with f being the switching frequency of the inverter.

Equation (3) shows that the output power of the IPT system is directly proportional to the secondary uncompensated apparent power, S_U, and the secondary-side loaded quality factor, Q_s

$$P_{\text{out}} = S_U Q_s. \tag{3}$$

According to (4), S_U can be obtained from the product of the receiver induced voltage, V_s, and the secondary short-circuit current ($I_{\text{SC}} = V_s / j\omega L_s$)

$$S_U = |V_s||I_{\text{SC}}| = \omega \frac{M^2}{L_2} I_p^2 = \omega \left(k^2 L_p\right) I_p^2. \tag{4}$$

From (3), the output power can be expressed as

$$P_{\text{out}} = S_U Q_s = \omega \left(k^2 L_p\right) I_p^2 Q_s = \omega \frac{M^2}{L_s} I_p^2 Q_s. \tag{5}$$

The power loss of the wireless charging system consists of the following components:
1) inverter losses (P_{inv});

2) resonant network losses (P_r);
3) magnetic coupler losses ($P_{coupler}$);
4) rectifier losses (P_{rec}).

The inverter losses are due to switch conduction loss and switching loss. The conduction loss of the inverter is dependent on the switch rms current and its ON-state resistance [25]. The switching loss is dependent on the modulation scheme, frequency, dc-link voltage, and rise and fall times of the switch. Different switching methods can be used to realize soft-switching, which results in the reduction of the switching losses [26]. Therefore, in the design stage of the wireless charging system, inverter VA should be minimized to reduce the inverter losses and reduces the implementation costs. The resonant network losses include the resonant capacitor losses and resonant inductor losses. The resonant capacitor losses can be calculated using the dissipation factor, and the resonant inductor losses include the conduction and core losses [27]. The magnetic coupler loss consists of the Litz wire losses, ferrite core loss, and aluminum shield loss [28]. In [29], a comparison of different magnetic couplers for EV wireless charging applications by defining a multiobjective optimization is presented. It was shown that, under misalignment conditions, a wireless charging system designed with a polarized magnetic coupler shows a better performance for the same power density [29]. Rectifier losses can also be calculated based on the conventional equations for a resonant converter presented in [30] and [31].

It can be seen in (5) that Q_s depends on the secondary compensation circuit, which can be connected in series, parallel, or a combination of both. Also, the equation implies that the transferred power is influenced by the operating frequency ω, the mutual inductance M, the transmitter current I_p, and the secondary quality factor Q_s. It is worth noting that ω and I_p can be controlled by the primary-side controller, and Q_s depends on the secondary compensation circuit, while M is uncontrollable within the charging process. When the relative position between the transmitter and the receiver changes, the mutual inductance M varies accordingly. If current I_p is kept constant, this will result in a reduction of output power and the system's efficiency. Consequently, the level of stray fields increases with potential harmfulness to the surrounding pedestrians and living animals. Therefore, various techniques have been proposed in the literature to address the effects of misalignment in the IPT system. Before discussing these techniques, a brief description of misalignment issues is first given. In general, two coils must be aligned so that the IPT system can achieve the best performance. However, this condition is rarely achieved in an EV wireless charger as the receiver is continuously moved along the transmitter (dynamic charging), or the receiver cannot be placed precisely as of the driver steering error. Coil misalignment refers to the condition where these two inductive coils do not maintain a relative distance equal to the one considered in the design process for any part constituting them. There are four main types of misalignments, namely, vertical, horizontal, the joint vertical–horizontal, and angular. Fig. 3 illustrates these misalignment types for square coils where it is also valid for other coil's shapes. The dimensions of the primary and secondary coils are

$a1 \times b1$ and $a2 \times b2$, respectively. It is noted that the primary coil is generally larger than the secondary one in practical EV wireless charger implementations.

In the vertical misalignment, the centers of the two coils (e.g., Center1 and Center2) are placed in a line perpendicular to the planes where the primary and secondary coils are present. In the design process of the coils, the centers of the coils are set to be separated at a certain distance equal to gd. If the vertical misalignment happens, this separation gap between two coils is varied. It could be greater or smaller than the design gap gd. Conversely, in the horizontal misalignment (in some documents referred to as lateral misalignment), the separation gap between two coils is maintained as gd. However, the centers are not aligned and the separation between Center1 and the reflection of Center2 in the plane of the primary coil is xm. Moreover, it is possible to occur simultaneously the vertical and horizontal misalignments, as illustrated in Fig. 3(c). Finally, angular or rotational misalignment [as shown in Fig. 3(d)] refers to the situation in which the two coils are not placed on two parallel planes where these planes containing the coils intersect with an angle β.

Since the placement of the vehicle may not be precise when initiating the wireless power transfer, coil misalignments in most cases are inevitable for EV wireless chargers. Lateral and vertical misalignments are typically considered in this kind of application. While lateral misalignment may occur because of an imprecise position of the EV, vertical misalignment is a consequence of different types of EV chassis, where the gaps between the chassis to the embedded primary coil are different. Angular misalignment has occurred more frequently in medical and consumer appliances rather than EVs chargers. To quantitatively the misalignment level, the standard SAE J2954 [20] defines three classes of the IPT system according to the separation gaps between two coils: Z1-class: gap between 100 and 150 mm; Z2-class: gap between 140 and 210 mm; and Z3-class: gap between 170 and 250 mm.

The misalignment tolerance requirements are set according to the offset direction. The maximum misalignment levels allowing for X- and Y-axes are ±75 and ±100 mm, respectively. For the Z-axis, the values are set, which depends on the different gaps defined in the Z-class above. The efficiencies targets for the EVs' wireless charger under misalignment conditions are also provided. SAE J2954 [20] sets the minimum target efficiencies at nominal alignment, and misalignments are 85% and 80% for all power levels, respectively. All above values are summarized in Table I. The last definition regards the angular misalignment, where the rotation of the vehicle around the X-axis (roll), the Y-axis (pitch), and the Z-axis (yaw) is limited to $\pm2°$, $\pm2°$, and $\pm10°$, respectively. Other international standards provided by the International Electrotechnical Commission (IEC) and the International Organization for Standardization (ISO), such as IEC 61890 [32] and ISO 19363 [11], also set similar restrictions on the misalignment.

The IPT charging systems for EVs usually experience output power pulsation under misalignment conditions. In order to achieve stable output power and high efficiency during misalignment, various design and optimization methods are
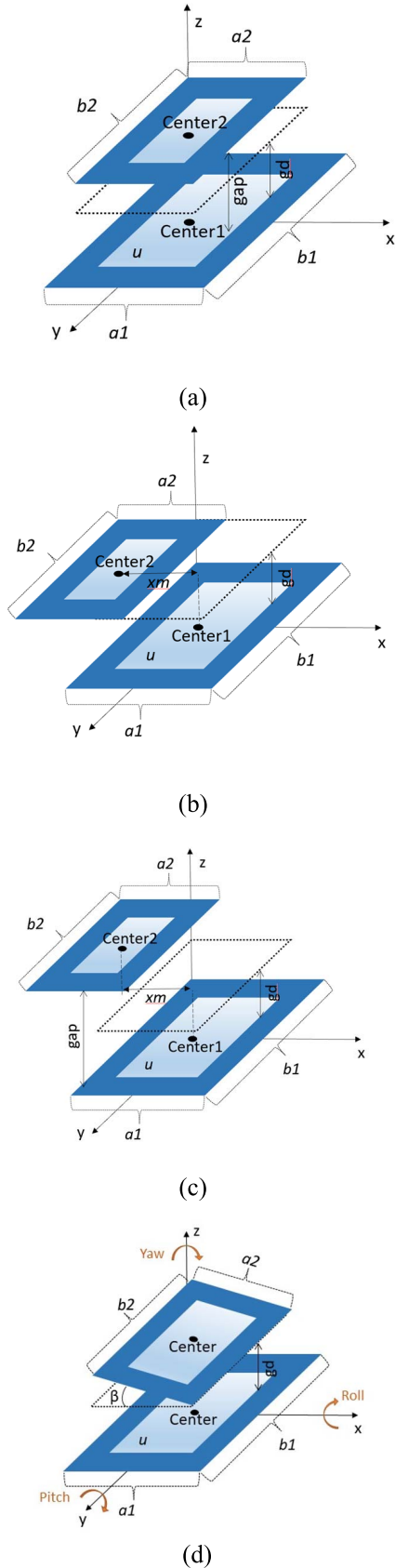
(a)

(b)

(c)

(d)

Fig. 3. Illustration of different types of coil misalignments that may occur in an EV wireless charger: (a) vertical misalignment, (b) horizontal misalignment, (c) vertical and horizontal misalignments, and (d) angular misalignment.

TABLE I
MISALIGNMENT RESTRICTION ON THE IPT CHARGER [20]

Charging power class [kVA]	WPT1	3.7
	WPT2	7.7
	WPT3	11.1
	WPT4	22
Separation gap [mm]	Z1-class	100-150
	Z2-class	140-210
	Z3-class	170-250
Vertical and horizontal misalignment [mm]	ΔX	± 75
	ΔY	± 100
	ΔZ^*	$Z_{nom}-\Delta_{low} \rightarrow Z_{nom}+\Delta_{high}$
Angular misalignment [°]	Roll	$\pm 2\%$
	Pitch	$\pm 2\%$
	Yaw	$\pm 10\%$
Minimum target efficiency [%]	At nominal alignment	>85% (for all power classes)
	Under misalignment	>80% (for all power classes)

Note: * Z_{nom} is nominal value depending on Z-class, Δ_{low} and Δ_{high} are the increments allowed in each Z-class.

proposed. Fig. 4 shows the detail of these methods that are classified into three main categories as follows:

1) methods based on the magnetic coupler coils;
2) methods based on control techniques;
3) methods based on topologies of the compensation tanks.

The main content of this article is also divided into different sections to address these categories. Section III elaborates on the dispensable part of the wireless charging system, e.g., the magnetic coupler, and focuses on how the coupler is designed to operate under the high misalignment condition. This article reviewed and classified the magnetic coupler layouts into two major groups, namely, single- and multiple-winding topologies. The diverse coil topologies presented in the literature present differences in the tolerance under misalignments; therefore, the suitability of a coil topology depends on the misalignment that the system must support. The coupling coefficient profile is required to be stable and high as much as possible during the charging process; as such, different design and optimization methods are proposed for the single-winding topologies to improve the performance. On the other hand, the multiple-winding topologies are preferable in cases where the misalignment occurs more often and in a large range, such as the EV dynamic wireless charging system. More windings in the same coupler create more coupling coefficients between the transmitter and receiver sides. These additional coupling coefficients are included to compensate for the reduction of the coupling between the original transmitter and the receiver.

Section IV provides a comprehensive study, analysis, and comparison of different compensation circuit topologies in
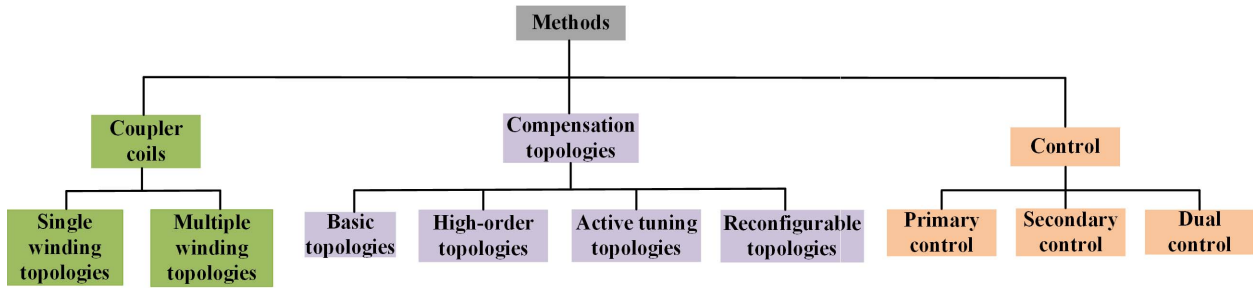
Fig. 4. Classification of the techniques for reducing the output power pulsation in IPT system for EVs.

terms of design and performance. The compensation circuit is an important part of the IPT system that reduces the reactive power and improves both the power transfer capability and the overall efficiency. The idea behind the compensation circuit is to cancel the high leakage inductances of the magnetic couplers with the aid of high-frequency compensation capacitors. These circuits are further categorized into four basic topologies, namely, series–series (S-S), series–parallel (S-P), parallel–series (P-S), and parallel–parallel (P-P) [4]. In order to simplify the control of IPT systems and reduce the sensitivity with the misalignment, high-order compensation topologies are proposed where resonant inductors are included in the compensation network. New topologies of active tuning and configuration are recently proposed to suppress the effects of the misalignment.

Section V deeply discusses the control techniques associated with the power converters of the wireless charger for EVs. The general aim of the control system is to achieve the required output power, voltage, and current under the variation of charging scenarios and misalignment conditions. Control algorithms are utilized to cope with misalignment not only to increase efficiency but also for safety reasons. When misalignment occurs, the currents flowing through the charger change their values and the control algorithm should adjust the operating point to improve the efficiency. Moreover, some variables of the system can exceed the maximum allowed values, and they must be verified by the algorithm. For high charging efficiency and sufficient protection, the constant current/constant voltage (CC/CV) mode is normally utilized with the vehicle battery. In this charging method, the vehicle battery is considered to be a variable load, which largely depends on the battery's State of Charge (SoC). The control system, therefore, needs to regulate the wireless charger output precisely to implement the CC/CV charging profile. Besides that, the control system also needs to maintain a good and stable efficiency during the charging process. There are three main control schemes for this purpose: duty cycle control, phase shift control, and frequency control. Depending on whether the control is performed at the primary side (off-board) or secondary side (onboard), the control methods are further classified into three: primary side, secondary side, or dual-side control. On the primary side, all three control schemes can be applied to the primary inverter. However, on the secondary side, a regulator of the dc/dc converter is often used with only the duty cycle control scheme. Dual-control is executed on the

primary and secondary sides. According to the new standard SAE J2954 [20] (i.e., wireless power transfer for light-duty plug-in/EVs and alignment methodology), the frequency band is recommended to be between 81.38 and 90 kHz with the main operating point at 85 kHz. Therefore, the operating frequency in real scenarios is also limited within this band (i.e., 81.38–90 kHz) when applying the frequency control method. To conclude this article, Section VI provides the main challenges and future developments, while some conclusions are drawn in Section VII.

III. MAGNETIC COUPLER TOPOLOGIES

The magnetic coupler (magnetic pad) is the key element of an IPT system. In most of the topologies, high-permeability ferrite core and aluminum plate are, respectively, used in guiding and shielding the magnetic flux of the magnetic couplers [22], [27]. Due to the eddy current effect and proximity effect, the ac resistance of the winding operating at high frequency will be increased compared to the wire dc resistance [33], [34]. At the high-frequency operation, the current tends to pass closer to the surface of the conductor known as the skin effect. Therefore, the effective cross-sectional area of the copper will be reduced as the frequency increases. To reduce the skin effect, smaller insulated strands of wire can be used, which is known as Litz wire [27]. In this case, the radius of each strand is selected to be smaller than the skin depth at the operating frequency [33]. The proximity effect also increases the ac resistance of the winding. When different turns of the coil are placed close to each other, the magnetic field generated by each turn displaces the current distribution in the other turn and vice versa. Therefore, the ac resistance will be increased. In order to mitigate the proximity effect losses, different types of the Litz wire with twisted bundles are used.

In [35], the Dowell method for calculating the ac resistance in a simplified model of a transformer is studied. Similarly, in [36] and [37], ac resistance calculation and optimal selection of the number of the strands in a transformer are presented. In [38], a comparison between conventional ac resistance calculation methods is presented. Although the magnetic structure of the wireless charging system is similar to a transformer, the coils are mainly surrounded by air in a magnetic coupler of a WPT system. Therefore, conventional methods to calculate the ac resistance cannot be used. In order to calculate the ac resistance for a loosely coupled transformer (LCT), finite element analysis (FEA) can be used. However,

these methods can be computationally expensive when the number of the strands increases [39]. Therefore, analytical methods are proposed to reduce the computation time [39], [40]. For instance, a combination of the FEA and partial element equivalent circuit (PEEC) to use the advantages of both methods is proposed in [41]. In this method, the FEA results based on the differential model are used to calculate the magnetic field distribution, and the integral formulation of Maxwell's equations is used to calculate the Litz wire losses. In [42], a frequency-dependent model for the losses of the Litz wire for wireless charging applications is presented.

A proper design of magnetic couplers results in a high coupling coefficient, high quality factors, and high tolerance with misalignment. These features lead to high efficiency and stable output power under misalignment conditions. In order to fulfill the above objectives, different magnetic couplers topologies are proposed in the literature and are categorized into two major groups.

1) *Single-Winding Topologies:* In this category, the magnetic coupler contains only one winding conductor. The common topologies under this category include circular, rectangular, and double-D (DD) topologies.

2) *Multiple-Winding Topologies*: In this category, the coupler coil contains more than one winding conductor, which results in more than one coupling coefficient. These topologies theoretically improve the tolerance under misalignment conditions. They enable capturing more flux components from different windings. Consequently, they provide higher tolerance to misalignment compared with the single-winding topologies.

In the following, the main coupler topologies of each category are discussed and analyzed.

A. Single-Winding Magnetic Coupler Topologies

The single-winding topologies are all classical and play an important role in the development of the IPT system. These topologies have been extensively reviewed in some previous works [1], and this article only provides a summary of their features. It has been established in the literature that different coil topologies with similar dimensions and material result in significantly different magnetic coupling effects and misalignment tolerance capabilities. Fig. 5 gives a summary of the basic single-winding coupler coil topologies in both static and dynamic inductive charging systems for EVs, while Table II gives a summary of their main features. To evaluate the performance of different coupler coil topologies, the fundamental flux path height of each topology is compared with the coil parameter, as summarized in Table II. Considering these features, an optimal design can be achieved depending on the type of application and the system specifications. In the case of EVs stationary charging systems, for example, circular and rectangular pads are widely used due to their simplicity in terms of structure and component count, thus minimizing the use of copper winding [22], [27], [43], [44]. However, these topologies exhibit poor performance in terms of low coupling coefficient and poor tolerance to misalignment. Several analyses [32] show that circular coils present a better
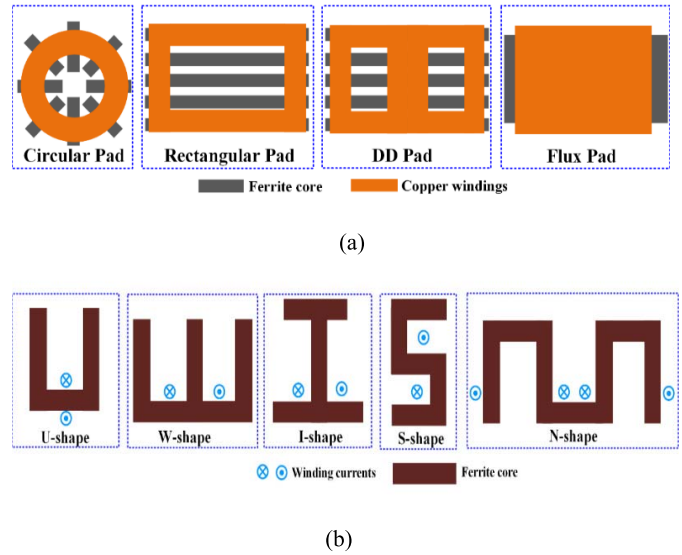

(a)

(b)

Fig. 5. Basic single-winding magnetic coupler topologies in IPT system for EVs. (a) Static wireless charging. (b) Dynamic wireless charging.

coupling factor compared with rectangular coils with similar dimensions. However, this convenience is only perceived when there is no misalignment. In fact, with misalignment, the variation of the coupling coefficient is greater in circular coils than the similar rectangular ones. To improve the magnetic coupler performance, a flux pile layout is proposed in [23] and [45]. Although higher coupling is realized, this topology results in a low-quality factor and a double-sided magnetic field effect. This causes unwanted losses and higher stray fields in the surrounding environment. In a similar development, a DD topology is proposed and used in [46]–[50]. This topology has the highest fundamental flux path height; it provides a better tolerance against misalignment and offers a high coupling coefficient [46], [47]. The DD coils also show superior performance to circular/rectangular topologies under the misalignment's occurrence, especially in the direction of the vehicle's movement. The coupling factor is reduced by only less than 50% with 50% misalignment on this axis. However, the shortcoming of this topology is the higher core losses incurred at the pad center, which has been analyzed and optimized in [50]. Furthermore, this topology suffers from the null-power issue, where the total magnetic field from the transmitter is canceled out at a certain level of horizontal misalignment on the receiver side [46]. A zero-coupling factor has occurred for a receiver's displacement of about 37% of the primary pad length. To overcome these limitations associated with the DD topology, different optimization techniques and design methods have continuously been proposed to achieve high misalignment tolerance, low stray field emissions, and improve system efficiency [48]–[50].

In the case of dynamic wireless charging where the EV could be charged while driving, the single-winding topologies are categorized into short-individual (segmented) transmitters [51]–[53], [60] and long-track transmitters [54]–[59] according to the length of transmitter coils. In the short-individual transmitters, the dimension of the transmitter is

TABLE II
SUMMARY OF THE MAIN FEATURES OF SINGLE-WINDING MAGNETIC COUPLER TOPOLOGIES

Topology in		Main Features	Pros	Cons	Applications
Transmitter	Receiver				
Circular/ Rectangular [22],[27],[43,44],[51]	Circular/ Rectangular	- Single-sided magnetic field. - The fundamental flux path height is equal to 1/4 of the coil diameter	- Minimum copper winding - Medium coupling coefficient	- Low misalignment tolerance	Static/dynamic charging
Flux pile/ solenoid [23],[45]	Flux pile/ solenoid	- Double-sided magnetic field - The fundamental flux path height is equal to 1/2 of the coil diameter	- High coupling coefficient - Medium misalignment tolerance	- Low quality factor with shielding presence	Static charging
Double-D [46-50],[52,53]	Double-D	- Single-sided magnetic field - The fundamental flux path height is equal to 1/2 of the coil diameter	- High coupling coefficient - Medium misalignment tolerance	- Higher core loss at the pad center - Null-power at a certain level of misalignment	Static/dynamic charging
W-shape [54]	Multiphase W-type	- Magnetic polarity of adjacent poles is unchanged. - Require reactive shielding	- Medium efficiency of 80% with 26-cm air-gap	- Large rail width (80-cm) - High stray field emission	Dynamic charging
U-shape [55,56]	Rectangular / Double-D or multiphase	- Magnetic polarity of adjacent poles is unchanged	- Medium efficiency of 72% at large air-gap of 17 cm	- Large rail width (72-cm) - High stray field emission	Dynamic charging
I-shape [57]	Double-D	- Magnetic polarity of adjacent poles is alternated. - Small rail width of 10 cm	- Very low stray field emission - Good tolerance with misalignment (typically 24 cm)	- High fluctuation of output power while driving - Low efficiency of 74% at 20-cm air-gap	Dynamic charging
S-shape [58]	Double-D	- Magnetic polarity of adjacent poles is alternated. - Very small rail width of 4 cm	- Very low stray field emission-Good tolerance with misalignment (typically 30 cm)	- High fluctuation of output power while driving - Low efficiency of 71% at 20-cm air-gap	Dynamic charging
N-shape [59]	Multiphase windings	- Magnetic polarity of adjacent poles is alternated. - Further reduce the volume of ferrite core compared to I-shape	-Very low stray field emission- Further reduce the ferrite volume and weight	- High fluctuation of output power while driving	Dynamic charging

similar to that of the receiver. The common classical topologies for the dynamic wireless charging system are circular [51] and DD magnetic couplers [52], [53], [60]. Multitransmitter coils are arranged on the primary side to alternately transfer power to the secondary side [51]–[53], [60]. In addition, each transmitter is connected to an independent compensation circuit. The power inverter on the primary side is usually shared by a set of transmitters connected in parallel. The transmitter coils are switched ON or OFF depending on the EV position [11]. In this way, the number of components and their corresponding costs are reduced. When the EV's receiver coil is aligned with a specific transmitter coil, then the power switch (typically, a contactor) connects the associated inverter. In order to switch a specific transmitter, position sensors and other associated electronic circuits are required. Therefore,

the effect of the electromagnetic field on the surrounding environment is minimized, and the total conduction losses on the transmitters are reduced. Moreover, higher efficiency can be achieved due to the higher values of the coupling coefficient between the transmitter and receiver coils, and lower conduction losses compared to the long-track transmitter [10]. In the case of the short-individual transmitter, the receiver covers entirely one transmitter coil surface. This leads to a higher coupling value compared to the long-track transmitter, where the receiver only covers a small portion of the transmitter length. However, the short-individual transmitters require more inverters, position sensors, and other control circuitries, thus making the system more complicated and costly [9], [10]. More importantly, when the EV moves between two adjacent transmitters, the coupling coefficients between two adjacent

transmitters and receivers reduce significantly; this results in an output power pulsating [61].

On the other hand, the long-track transmitters [54]–[59] are much longer than the EV length and only require a single power inverter with one compensation tank, making the system simpler and cheaper. The single-winding topology is named after the ferrite core shape of the long-track transmitter. However, the low coupling coefficient is recognized as the main drawback of this system because the receiver coil covers only a small portion of the long transmitter coil. This results in a lower efficiency profile and higher stray magnetic fields. Several studies are conducted to address the problems associated with the stray fields and also to simplify the design of magnetic shielding [57]–[59]. For example, in [57] and [58], I- and S-type transmitters are proposed with a width of 10 and 4 cm, respectively, to further reduce the transmitter coil width. Furthermore, stray fields can be substantially reduced if the magnetic polarities of adjacent poles are alternated [57]. In another development, an N-type transmitter is proposed in [59] to further reduce the volume of the ferrite core while maintaining the advantages of the I-type structure. However, further studies show that the magnetic flux density generated by I-, S-, or N-type transmitters on a single receiver varies in a nearly sinusoidal function, depending on the receiver's position along the driving direction. According to Huh *et al.* [57], the magnetic flux density reaches its maximum value at the center of each ferrite pole and reduces to nearly zero at the center between two adjacent poles. Consequently, the induced voltage and received power are significantly varied depending on the position of the EV. In fact, the received output power even reaches nearly zero at some specific positions of the EV while moving along the transmitter.

B. Multiple-Winding Magnetic Coupler Topologies

Utilizing multiple windings for the magnetic couplers has the following purposes in EVs' wireless charging:

1) improving misalignment tolerance and reduction of the output power variation;
2) achieving higher transmission efficiency;
3) improving the power density by integrating compensation components with the magnetic couplers.

This section extensively reviews different types of magnetic coupler topologies for each of the above purposes.

1) Improving Tolerance With Misalignment: In order to further improve the misalignment tolerance of the IPT system, more windings are added on either one side or both sides of the IPT system. The main principle is that more coupling coefficients (i.e., mutual inductances) are included to compensate for the coupling reduction between the original transmitter and the receiver under misalignment conditions. As a result, more than one induced voltage is shown up on the receiver from the transmitter's side. This guarantees more stable output power. This method can be further classified into: 1) multiple transmitters; 2) multiple receivers; and 3) multiple transmitters and receivers, depending on where the additional copper windings are added. The overall structure of the multiple-winding IPT system is shown in Fig. 6. The primary magnetic
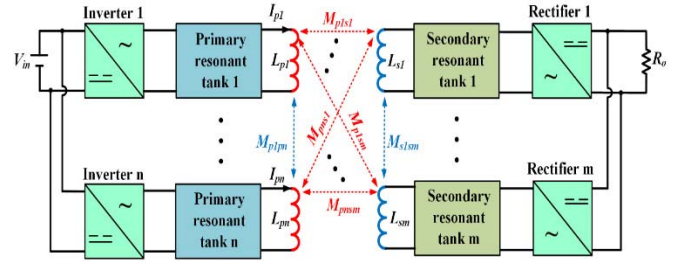

Fig. 6. Overall structure of the multiple-winding IPT system.

couplers include n windings (namely Lpi, $i = 1, n$), while the secondary magnetic couplers consist of m windings (namely Lsj, $j = 1, m$). One receiver winding Lsj will couple with n transmitter windings Lpi ($i = 1, n$), where the mutual inductances are $Mpisj$ ($i = 1, n$). If each transmitter winding Lpi is supplied by a current source Ipi ($i = 1, n$), the total induced voltage Vsj on the receiver winding Lsj is calculated as [61]

$$V_{sj} = j\omega \sum_{i=1}^{n} M_{pisj} I_{pi}. \tag{6}$$

It can be seen from (6) that the additional mutual inductances $Mpisj$ ($i = 2, n$) help to stabilize the induced voltage V_{sj} under misalignment scenario when $Mp1sj$ is reduced. Therefore, these topologies have the advantage of providing higher tolerance to misalignment conditions. Moreover, they can also supply a higher power level to the load compared to the single-winding topology of the same power rating.

However, there are two main disadvantages of using multiple-winding topologies. First, the aforementioned benefits come at the expense of higher cost and larger space requirements; as such, only two or three windings are normally used to minimize the cost [46], [47]. Second, there exist cross-mutual inductances between the transmitter and receiver windings [62], [63]. These inductances cause higher current stresses through the inverter switches and the resonant tanks, and can lead to destructive effects on the inverter switches. There are two common methods for compensating the effects of the crossing mutual inductances. In the first method, different windings on one side are arranged to mutually decouple from each other [64]–[68]. In the second method, the compensation capacitor is connected in series with each transmitter/receiver winding to alleviate the induced voltages caused by the cross-coupling [61]. Different topologies are reviewed as follows.

a) DDQ topology: The double-D quadrature (DDQ) coupler is developed from the DD coil (receiver side) by adding an extra quadrature winding, which is mutually decoupled from the existing DD winding [46], as shown in Fig. 7(a). The DD topology yields a power null point when the horizontal misalignment is around 34% of the pad length [46]. Under this condition, the total flux from the transmitter winding is canceled, resulting in no induced voltage on the receiver winding. The additional Q winding helps to avoid this issue by introducing an additional coupling coefficient to the transmitter
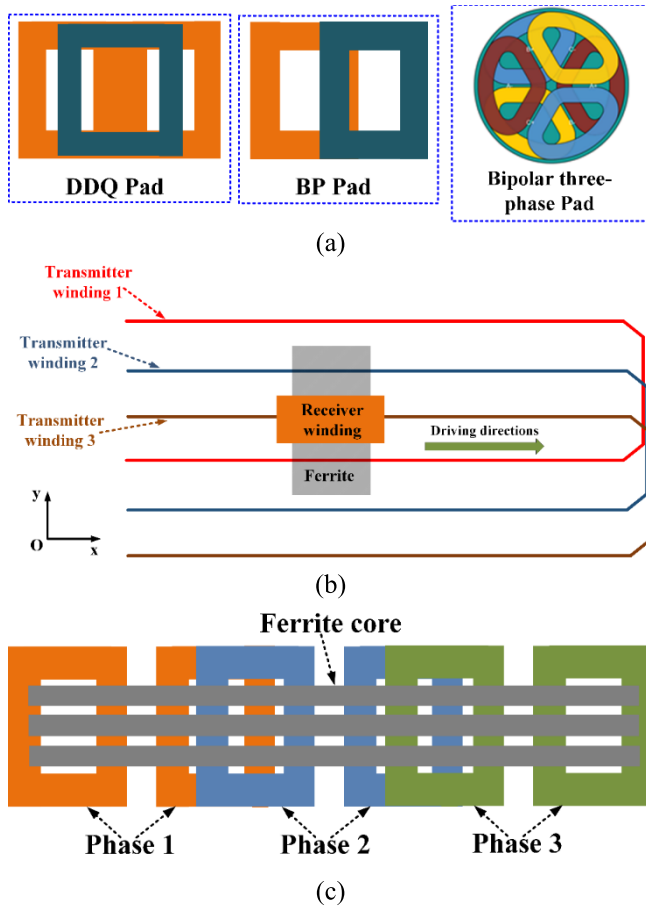
(a)

(b)

(c)

Fig. 7. Different multiple-winding topologies for EVs' wireless charging. (a) In stationary charging: DDQ pad [46], BP pad [64], [65], and bipolar three-phase pad [62]. (b) Three-phase transmitter for dynamic charging [70]. (c) Three-phase receiver for dynamic charging [71].

coil. The tolerance to the misalignment of primary-DD and secondary-DDQ pads significantly improves by providing a charge zone that is three times larger than the conventional DD topology and five times larger than the circular topology when a similar volume of materials is used [46]. The DDQ topology is mostly used on the receiver side, while the DD topology can be used either on transmitter or receiver sides [3], [16]. The combination of the DD coil on the transmitter side and DDQ on the receiver side is commonly used for high air-gap applications [46]. The DDQ topology shows better interoperability compared to the DD topology, where DDQ can interoperate well with many types, including the circular pad.

b) Bipolar pad topology: In order to reduce the copper winding usage while maintaining the same performance as with the DDQ pad, the bipolar pad (BP) is proposed in [64] and [65]. There are two identical windings, which are partially overlapped and mutually decoupled in one transmitter or receiver pad, as shown in Fig. 7(a). While the BP topology maintains the same level of high misalignment to tolerance and high coupling coefficient, it also saves up to 27.7% of copper compared to the DDQ topology [65]. The BP topology can be used on either transmitter or receiver side and with

the high air-gap applications [16], [69]. This topology owns good interoperability when combined with different types of receivers, such as circular or DD pads [69].

c) Tripolar pad topology: Based on the partial overlap concept of the BP topology, the tripolar pad (TPP) topology on the transmitter side has been proposed in [66] and [67]. In this configuration, one transmitter pad incorporates three identical windings, which are also partially overlapped and mutually decoupled. The main advantage of this topology is that it results in higher rotational misalignment tolerance compared with the other topologies, such as DD, DDQ, and BP. Each winding is independently controlled by an inverter in the tripolar topology. The effective mutual inductance to the secondary pad can be maximized by controlling the amplitude and phase of each primary winding current. The receiver topologies of circular and bipolar are interoperable with the TPP transmitter. Besides the rotational misalignment, the TPP topology shows a very high tolerance with misalignment when BP is adopted as the receiver pad. However, this comes with a price of a complex control algorithm. This topology can be also used in both transmitter and receiver sides in high air-gap applications [16].

d) Bipolar three-phase topology: To improve the power density for high-power EV wireless charging systems, Pries *et al.* [62] proposed a bipolar three-phase topology with rotating magnetic fields, as shown in Fig. 7(a). In this topology, each phase includes two individual windings arranged in opposite polarity in such a way that the flux created by one winding returns through its associated winding of the same phase. This feature is similar to the DD or BP topologies. In contrast to the approach in [66] and [67], the three-phase windings proposed in [62] are placed in overlapped passion and are also equipped with cross-mutual inductances between them. The main purpose of this topology is to improve the power density by maximizing the power transfer while minimizing the pad dimension. Compensation capacitors are tuned properly to address the effect of the crossing mutual inductances. This topology is capable of sustaining the rotational misalignment such that the output power and efficiency remained unchanged for 30° of misalignment. However, it heavily suffers from vertical/horizontal misalignment; in that case, the output power drops to nearly 80% under the vertical/horizontal misalignment of 10/10 cm [62].

e) Multiphase windings for dynamic charging: Misalignment level is always higher in the dynamic charging system compared to the stationary counterpart. Therefore, proper selection of coil topology and careful design are always required to provide a better tolerance with misalignment. In addition to the misalignment challenge, the transferred power of a single-phase dynamic charging system is limited by voltage and current ratings of the semiconductor devices, transmitter coil, and compensation circuits. In real applications, several EVs may need to be charged simultaneously with different power levels; thus, the high-power demand becomes a necessity. Therefore, the primary side of the dynamic charging system must be able to provide the highest power demand to meet these requirements. Multiphase systems can help to address these issues. Generally, the multiphase systems

achieve, more easily, a near-uniform magnetic field distribution compared to the single-phase system. This partially releases the misalignment effect and helps to achieve more stable output power. Therefore, multiphase windings systems are utilized more frequently in dynamic charging compared to stationary charging [61].

In order to achieve a stable output power, the amplitude and phase of the transmitter's current are regulated depending on the coupling factor profile. Numerous multiphase IPT systems have been studied in the literature. These systems vary greatly in terms of magnetic coupler topologies and the associated power electronic components. An analysis was conducted in [61] to determine the conditions of the phase and amplitude of each winding's current for achieving constant output power in the driving direction. Detailed design and analysis of two- and three-phase transmitters based on I-shape are also studied in [68] and [72]. To further reduce the cost and weight of the transmitter, the ferriteless three-phase IPT systems are proposed in [70], [73], and [74]. Fig. 7(b) and (c) illustrates the examples of multiphase transmitter and receiver in dynamic charging.

However, the obvious downside of using a multiphase windings transmitter is the requirement of higher copper winding and associated cost. It was established in [61] that the I-shape topology based on two- and three-phase transmitter systems, respectively, requires two and 2.5 times higher copper length compared to the single-phase system. Therefore, numerous studies propose the multiphase receivers on the vehicle side while using the single-phase transmitter [54], [63], [71], [75]–[79]. Similar to multiphase transmitter IPT systems, the multireceiver system includes multiple windings working independently on the vehicle side. These windings simultaneously couple with one or several transmitter winding(s), while the EV is in motion. The additional windings can be either included in a vertical or horizontal direction depending on which direction the misalignment occurs more often. The phase output terminals can be connected as series or parallel depending on the vehicle battery's requirement, which is either high voltage or high current.

2) Achieving Higher Conversion Efficiency: Another purpose of utilizing the multiple coil windings is to improve the effectiveness of the coupling coefficient and extend the energy transfer distances. This method utilizes some additional windings, commonly known as intermediate coils, along with existing transmitter and receiver coils [80]–[83]. The intermediate coils are not connected to any power electronic circuit, such as an inverter or a rectifier; instead, they are connected through a resonant capacitor. The idea is to boost the apparent coupling coefficient of the system at the operating frequency while keeping the same coupling coefficient between the transmitter and receiver coils. It was reported in [83] that a two-intermediate coil system achieves an efficiency of 97.1% with a 20-cm air gap even without using a ferrite core. However, the design technique for this kind of system is more complex than that of the conventional two-coil IPT system. Fig. 8 shows different topologies based on intermediate coils, namely, topology with only one intermediate coil in the transmitter circuit [80], [81], topology with two intermediate
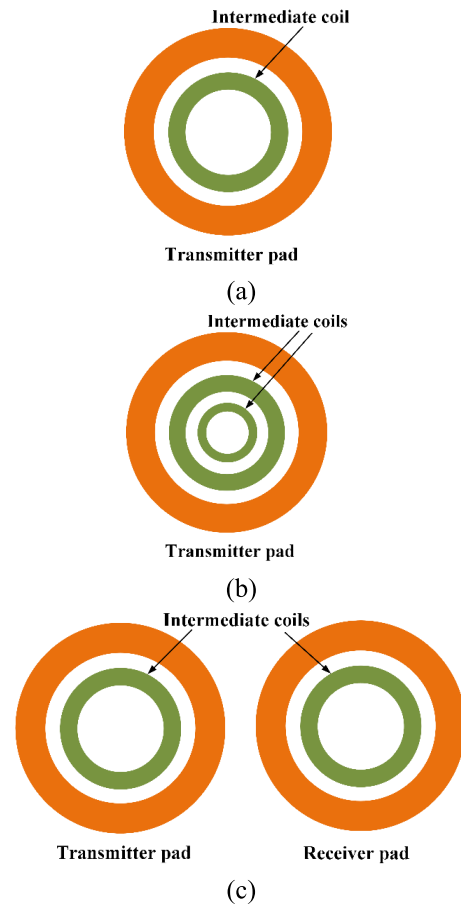

Fig. 8. Different topologies using the "intermediate coils" concept. (a) One coil on the transmitter side [80], [81]. (b) Two coils on the transmitter side [82]. (c) One coil on both transmitter and receiver sides [83].

coils [82], [83], and topology with one intermediate winding on either transmitter side [80]–[82] or both transmitter and receiver sides [83]. The intermediate coil is normally designed with a circular pad because of its lower coupling coefficient than DD and BP pads.

It is worth noting that this approach to achieving higher conversion efficiency is more commonly used in stationary charging systems where the misalignment level is typically lower than that of a dynamic charging system. Nevertheless, the concept is still applicable to the dynamic charging system but with a more complicated design procedure, especially when the coupling coefficient varies in a wide range.

3) Integrating Compensation Components With the Magnetic Couplers: In addition to the coupler, other coils may be used in a wireless charger. Higher order compensation topologies, such as double-sided *LCC* or *LCL*, require large resonant inductors on both the transmitter and receiver sides. In addition, the back-end dc/dc converter is, sometimes, required on the receiver side to regulate the output voltage for implementing CV and CC profiles for the vehicle's battery. This converter always demands a bulky inductor, which increases the weight and volume of the system. To overcome this issue, the idea of integrating these inductors into the main couplers has been proposed in [84]–[89]. For example, in [84]

and [85], the two resonant inductors of the double-sided *LCC* tanks were integrated with the main coupler, thereby reducing the size of the system. There are a total of four windings in the system, but the integration results in having five cross-coupling coefficients as these windings are placed close together, thus complicating the design parameters. To eliminate the cross-coupling coefficients, Kan *et al.* [86], [87] integrate the bipolar inductor coils with the unipolar main magnetic couplers. In another development, Ramezani and Narimani [88], [89] integrate the back-end converter's inductor as a bipolar coil into the main coupler unipolar coil.

In contrast, Vu *et al.* [90] and Mohamed and Mohammed [91] proposed a hybrid charging system of the inductive–conductive system where two transformer windings in the conductive converter are utilized as dual receivers in the inductive charging. This approach maximizes the sharing of both poof tower electronic and magnetic components on the vehicle side. Fig. 9 presents some integration winding topologies in IPT systems.

Table III gives a summary of the comparison of the characteristics of different multiple-winding pad topologies. In particular, the comparison established a summary of the behavior of the pads in terms of the following features:

1) interoperability;
2) charging zone (appropriate side);
3) leakage flux (safety degree);
4) suitable side (transmitter or receiver);
5) air gap (distance);
6) compatibility with static or dynamic charging;
7) tolerance of misalignment;
8) flux path.

IV. COMPENSATION NETWORKS

The wireless coupler or LCT of an IPT system absorbs a large value of reactive power due to the large leakage inductances [5]. As such, it is essential to compensate for the reactive power of the magnetic couplers by using resonant topologies in the IPT systems. The main purpose of the resonant circuit in the IPT system is to compensate for the high reactive power of the LCT. The resonant circuits offer interesting features, such as soft switching, high efficiency, high power density, and flexible output voltage/current [6].

A. Requirements and Challenges

Misalignment of the magnetic couplers results in deviation of the coupling factor, k, from the nominal value, which results in variation of the input impedance, input phase angle, output power, and efficiency of the system. Therefore, it is essential to design the resonant network properly in order to keep the efficiency as high as possible and to achieve a constant power (CP), CV, or CC in the output by reducing the output sensitivity to coupling factor variation [28]. The number of the resonant elements and safe operation of the transmitter side converter in the case of the absence of the receiver coil is also a requirement in a dynamic charging application to avoid damaging the inverter and the resonant elements. The requirements, such as achieving high efficiency and reduction
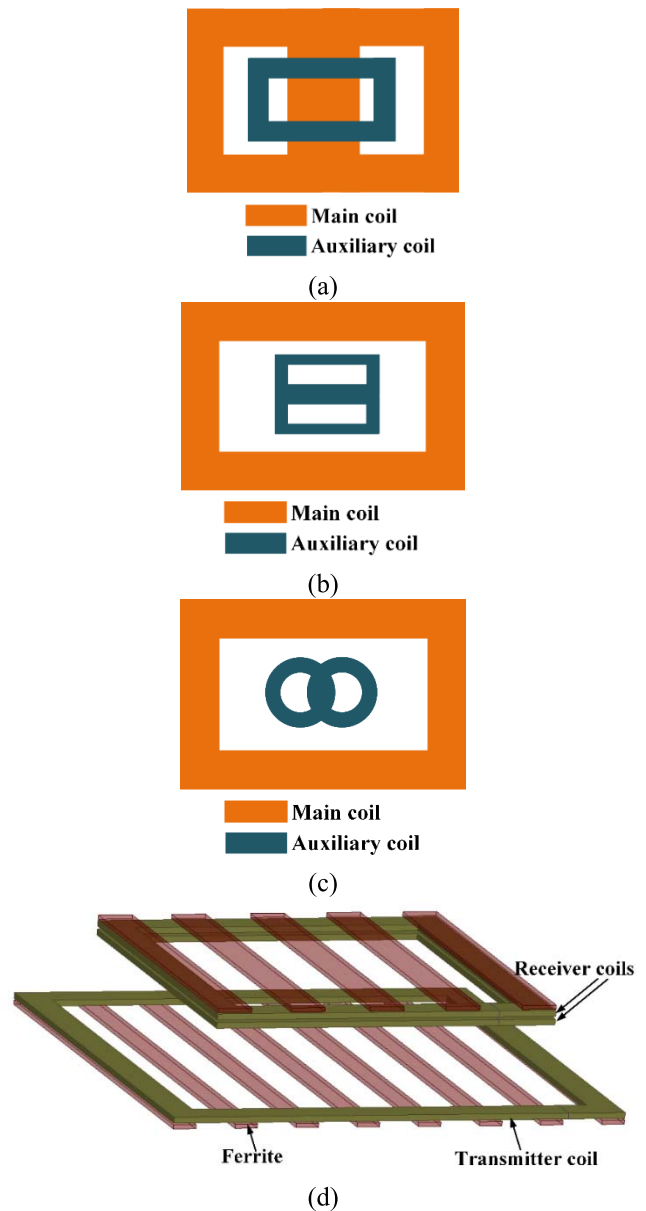

(a)

(b)

(c)

(d)

Fig. 9. Different integration topologies using multiple windings in the IPT system. (a) Main coil: bipolar, auxiliary coil: unipolar [86]. (b) Main coil: unipolar; auxiliary coil: bipolar (double-D) [87]. (c) Main coil: unipolar; auxiliary coil: bipolar (double circular) [88], [89]. (d) Two receiver windings integrated from the conductive mode [90].

of the output sensitivity to misalignment, should be considered in the selection and designing of the resonant networks for a misalignment-tolerant wireless charging system.

B. Topologies

Generally, the structure of the resonant topologies can be divided into three groups, as shown in Fig. 10. In each circuit, the voltage gain, G_v, is defined by the ratio of the output voltage V_o to the input voltage V_{in}. Input impedance, efficiency, and output voltage gain ($G_v = V_o/V_{in}$) are the key parameters that need to be defined for analyzing each resonant topology. The input impedance can be used to calculate the input phase angle, input current, and voltage gain as a function

TABLE III
CHARACTERISTICS COMPARISON OF MULTIPLE-WINDING PADS

Pad topology	Double D quadrature	Bipolar	Tripolar	Multiphase	Bipolar three phase	One-intermediate on transmitter	Two-intermediate on transmitter	One-intermediate on each side
Interoperability	High	High	High	Medium	Low	Medium	High	High
Charging zone	Large	Large	Large	Dependent	Large	Medium	Large	Large
Leakage flux	Very low	Very low	Low	Low	Low	Low	Medium	Medium
Suitable side operation (transmitter or receiver)	Receiver	Both	Both	Transmitter	Both	Transmitter	Transmitter	Both
Airgap	High	High	High	Medium	Medium	Small	High	Medium
compatibility with static/ dynamic	Both	Both	Static	Both	Static	Static	Static	Static
tolerance of misalignment	High	Medium	High	High	High	Medium	High	High
Flux path	Double sided	Double sided	Single sided	Dependent	Double sided	Single sided	Single sided	Single sided
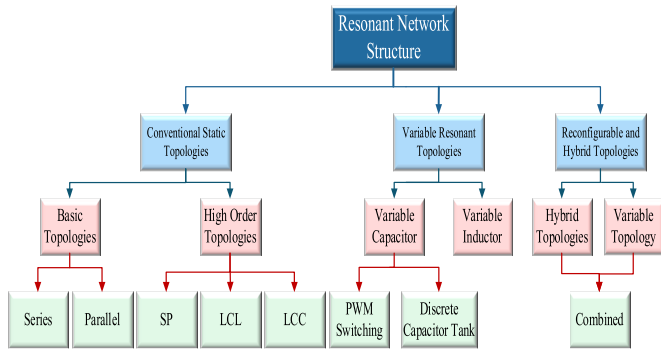
Fig. 10. Resonant network structures for IPT systems.

of the resonant elements. However, it is anticipated that, in a misalignment-tolerant topology, the efficiency and voltage gain should have less dependency on the coupling factor. Table IV gives a summary of the schematic of the commonly used topologies, their output voltage gain, and their input impedances.

The reflected impedance, Z_r, is defined as

$$Z_r = \frac{(M\omega)^2}{Z_{sec}} \quad (7)$$

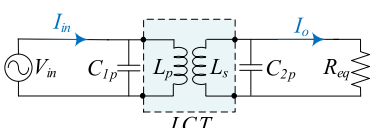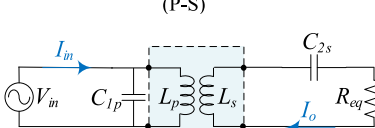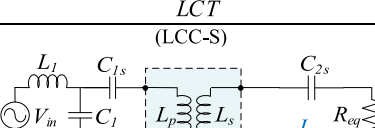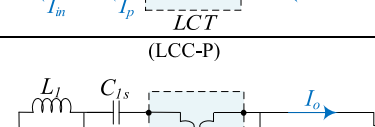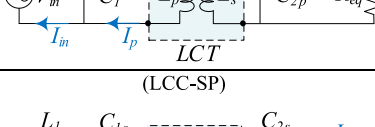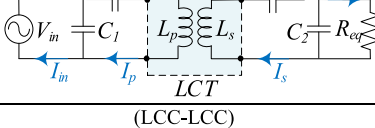where Z_{sec} is the impedance of the secondary-side circuit.
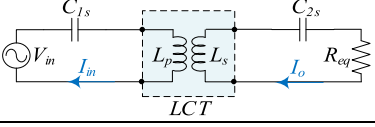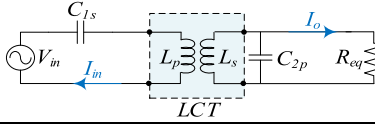
Next, some of the common compensation topologies and their design challenges in terms of misalignment tolerance capability are studied.

1) Basic Topologies: Four basic topologies that can be obtained using a single resonant element on each side of the LCT include S-S, S-P, P-P, and P-S topologies. However, the S-S topology is more commonly used in most applications due to its simplicity in the design, low component count, and high efficiency at the nominal operating point [92]–[96]. Generally, topologies with a series configuration on the primary side (typically S-S and S-P) have their input current being unbounded, necessitating the need for a protection circuit [6], [97], [98]. In these topologies, the input impedance phase angle is highly dependent on the load and coupling conditions. They are highly sensitive to misalignment and, therefore, unsafe for operation under such conditions [6], [99].

Compared to series primary-side compensation, the primary side of parallel-compensated systems (typically P-S and P-P) configurations can operate safely without the receiver coil. Generally, topologies with a parallel compensation on the secondary side suffer from excessive output voltage at light-load conditions [31] and are highly sensitive to the misalignment of the magnetic couplers [97]. Moreover, the P-P topology suffers from a low input power factor as seen by the inverter [6], and its output power depends on the mutual inductance [100].

In summary, all the basic topologies are not suitable for a misalignment-tolerant inductive charging system. In the absence of the receiver coil, both primary and secondary sides are unsafe under high misalignment or light load conditions. Moreover, by having a limited number of components,

TABLE IV

VOLTAGE GAIN AND IMPEDANCE DEFINITION OF DIFFERENT CONVENTIONAL RESONANT TOPOLOGIES

Topology schematic	Voltage Gain (G_v)	Impedances
(S-S)	$\dfrac{M\omega R_{eq}}{\lvert Z_{in}\rvert\lvert Z_{\sec}\rvert}$	$Z_{in} = \dfrac{1}{j\omega C_{1s}} + j\omega L_p + Z_r \quad Z_{\sec} = j\omega L_s + \dfrac{1}{j\omega C_{2s}} + R_{eq}$
(S-P)	$\dfrac{M\omega R_{eq}}{\left\lvert 1 + j\omega C_2 R_{eq}\right\rvert\lvert Z_{in}\rvert\lvert Z_{\sec}\rvert}$	$Z_{in} = \dfrac{1}{j\omega C_{1s}} + j\omega L_p + Z_r$ $Z_{\sec} = \left(R_{eq}^{-1} + j\omega L_s^{-1} + j\omega C_{2p}\right)^{-1}$
(P-P)	$\dfrac{M\omega R_{eq}}{\left\lvert 1 + C_1\omega\left(Z_r + j\omega L_p\right)\right\rvert\left\lvert 1 + j\omega C_2 R_{eq}\right\rvert\lvert Z_{in}\rvert\lvert Z_{\sec}\rvert}$	$Z_{in} = \left(j\omega C_{1p} + \dfrac{1}{j\omega L_p + Z_r}\right)^{-1}$ $Z_{\sec} = \left(R_{eq}^{-1} + j\omega L_s^{-1} + j\omega C_{2p}\right)^{-1}$
(P-S)	$\dfrac{M\omega R_{eq}}{\left\lvert 1 + C_1\omega\left(Z_r + j\omega L_p\right)\right\rvert\lvert Z_{in}\rvert\lvert Z_{\sec}\rvert}$	$Z_{in} = \left(j\omega C_{1p} + \dfrac{1}{j\omega L_p + Z_r}\right)^{-1}$ $Z_{\sec} = j\omega L_s + \dfrac{1}{j\omega C_{2s}} + R_{eq}$
(LCC-S)	$\dfrac{M\omega R_{eq}}{\left\lvert 1 + C_1\omega\left(Z_r + j\omega L_p - \dfrac{j}{\omega C_{1s}}\right)\right\rvert\lvert Z_{in}\rvert\lvert Z_{\sec}\rvert}$	$Z_{in} = j\omega L_1 + \left(j\omega C_1 + \left(j\omega L_p - \dfrac{1}{j\omega C_{1s}} + Z_r\right)^{-1}\right)^{-1}$ $Z_{\sec} = j\omega L_s + \dfrac{1}{j\omega C_{2s}} + R_{eq}$
(LCC-P)	$\dfrac{M\omega R_{eq}}{\left\lvert 1 + C_1\omega\left(Z_r + j\omega L_p - \dfrac{j}{\omega C_{1s}}\right)\right\rvert\left\lvert 1 + j\omega C_2 R_{eq}\right\rvert\lvert Z_{in}\rvert\lvert Z_{\sec}\rvert}$	$Z_{in} = j\omega L_1 + \left(j\omega C_1 + \left(j\omega L_p - \dfrac{1}{j\omega C_{1s}} + Z_r\right)^{-1}\right)^{-1}$ $Z_{\sec} = \left(R_{eq}^{-1} + j\omega L_s^{-1} + j\omega C_{2p}\right)^{-1}$
(LCC-SP)	$\dfrac{M\omega R_{eq}}{\left\lvert 1 + C_1\omega\left(Z_r + j\omega L_p - \dfrac{j}{\omega C_{1s}}\right)\right\rvert\left\lvert 1 + j\omega C_2 R_{eq}\right\rvert\lvert Z_{in}\rvert\lvert Z_{\sec}\rvert}$	$Z_{in} = j\omega L_1 + \left(j\omega C_1 + \left(j\omega L_p - \dfrac{1}{j\omega C_{1s}} + Z_r\right)^{-1}\right)^{-1}$ $Z_{\sec} = \left(R_{eq}^{-1} + \left(\left(j\omega C_{2s}\right)^{-1} + j\omega L_s\right)^{-1} + j\omega C_{2p}\right)^{-1}$
(LCC-LCC)	$\dfrac{M\omega R_{eq}}{\left\lvert 1 + C_1\omega\left(Z_r + j\omega L_p - \dfrac{j}{\omega C_{1s}}\right)\right\rvert\left\lvert 1 + C_2\omega\left(R_{eq} + j\omega L_2\right)\right\rvert\lvert Z_{in}\rvert\lvert Z_{\sec}\rvert}$	$Z_{in} = j\omega L_1 + \left(j\omega C_1 + \left(j\omega L_p - \dfrac{1}{j\omega C_{1s}} + Z_r\right)^{-1}\right)^{-1}$ $Z_{\sec} = \left(\left(R_{eq} + j\omega L_2\right)^{-1} + \left(\left(j\omega C_{2s}\right)^{-1} + j\omega L_s\right)^{-1} + j\omega C_{2p}\right)^{-1}$

their flexibility is not good enough for achieving multiple objectives [28].

2) High-Order Topologies: LCL and *LCC* resonant topologies are extensively used in the primary side of the IPT systems to supply the transmitter coil with a CC, which induces a CV on the secondary-side coil. The *LCC* network is commonly used instead of the *LCL* topology since it offers more degree of freedom for the designers to achieve the desired characteristics [101]. In the *LCC* topology, the constant amplitude of the primary-side current is independent of the load and mutual inductance, and it can be achieved by a smaller resonant inductor compared to the *LCL* topology [102], [103]. Moreover, safe operation of the inverter in the case of misalignment and improvement of light load efficiency can be achieved [104]. The *LCC*-based topologies, such as *LCC*-S [105]–[108], the *LCC*C-S [109], the *LCC*-SP [110], the *LCC*-P [111], [112], and the *LCC–LCC* [113]–[117], are widely used in the IPT application due to its suitable
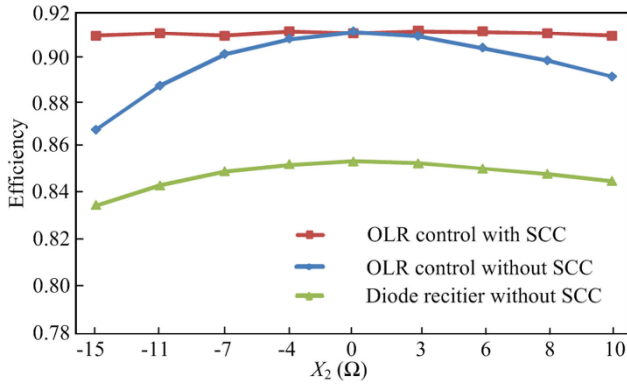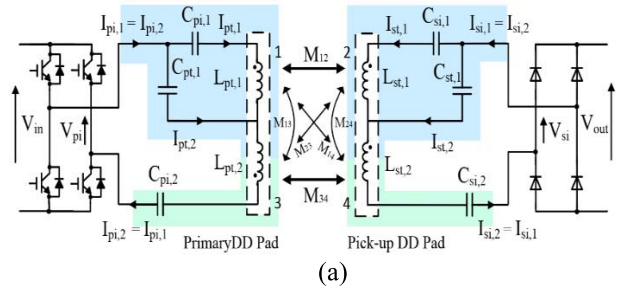
Fig. 11. Combination of the SCC and dual-side control method [125].

Fig. 12. Schematics of the hybrid and reconfigurable topologies. (a) Series-hybrid topology [126]. (b) Reconfigurable topology [127]. (c) Combination of the SCC and dual-side control method [130].

performance. Although the *LCC*-P topology has a constant output current behavior, zero phase angle (ZPA) switching is not achievable [112]. In contrast, the *LCC*-S topology can be designed to supply the load as a CV source independent of the load [25]. At the resonant frequency, the *LCC–LCC* topology converts the CV of the input to a CC in the output of the system [99]. It can also achieve both CV and CC modes if the resonant elements are tuned for two different resonant frequencies [117]. The *LCC–LCC* topology has outstanding performance compared to other topologies. However, due to a large number of components' counts, the power density and efficiency of the system are low. To reduce the number of components and increase the power density, integrated magnetic structures are proposed [84]. For instance, in [84]–[87] and [118], the resonant inductors of a dual-side *LCC* compensation topology are integrated with the main magnetic couplers to save ferrite material and reduce the converter volume.

3) Active Tuning: In general, the self-inductances of the magnetic couplers are also changed when misalignment occurs, which results in lower efficiency and variation in the voltage gain of the system. In [119], a variable-tuning *LCL* converter and an active variable inductor implementation are introduced. A similar approach is used in [120] and [121] to address the misalignment issue of the IPT system. In this method, the primary-side resonant inductor of the *LCC* network is considered a variable inductor to keep the inverter at the optimal switching point.

Another method of implementing active tuning of the resonant network is by using switching-controlled capacitors [122]. In [123] and [124], a fixed size capacitor is switched in pulsewidth modulation (PWM) mode to form a variable capacitor, e.g., C_{eq}. In [125], however, a dual-side control with online mutual inductance estimation is implemented, in which the output voltage is regulated by the inverter. An active rectifier is also used to ensure maximum power delivery. Fig. 11 shows a comparison of the efficiencies of a regular diode-bridge pickup converter (green), a dual-side controlled system (blue), and the switched-controlled capacitor (red). In Fig. 11, X_2 represents the equivalent reactance of the receiver side ($X_2 = \omega L_2 - (1/\omega C_{eq})$) [125]. It can be realized that there is a significant difference in the optimal
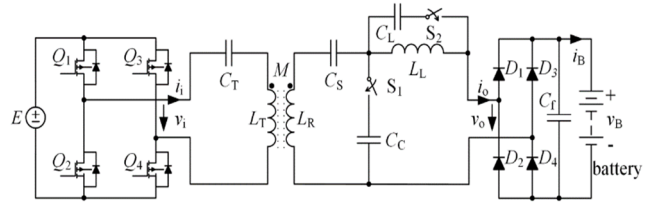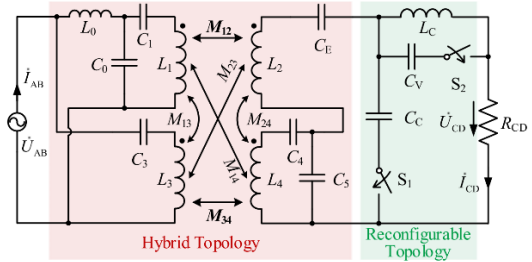
load resistance (OLR) control with and without a switched controlled capacitor (SCC).

4) Hybrid and Reconfigurable Topologies: Hybrid topologies combine the benefits of each topology and gain a robust system against coupling factor variation. For instance, series and *LCC* topologies can be combined in both the transmitter and the receiver of the IPT system to provide a CP over a wide range of misalignment [126]. The schematic of this topology is shown in Fig. 12(a). In such a system, as the misalignment level increases, the reflected impedance of the series-compensated transmitter circuit reduces while increasing the reflected impedance to the *LCC*-compensated transmitter circuit. Therefore, the input current of the series compensation branch will be increased inherently, and the total transmitted power to the secondary side will remain constant.

Instead of continuous tuning of the resonant network, a reconfigurable topology can also be used. In this method, the resonant topology is switched depending on the operating condition. The schematic of this method is illustrated in Fig. 12(b). Compared to the SCC method, the reconfigurable topologies do not require a PWM switching of the resonant elements. Thus, control complexity and cost will be reduced. In [127], a reconfigurable topology is proposed which switches between S-S and S-*LCC* to implement CC and CV modes,

TABLE V
COMPARISON OF DIFFERENT RESONANT STRUCTURES

Structure	Resonant Elements	Auxiliary Circuits	Flexibility	Complexity of Control
Basic Topologies	Lowest number of elements (only capacitor).	No	Low	Simple
High order topologies	Medium number of elements (capacitor and inductor)	No	Medium	Simple
Active Tuning	At least one variable inductor or capacitor	Yes	Medium	High
Hybrid and Reconfigurable Topologies	Highest number of elements	Yes	High	Medium

Fig. 13.   Tuning methods of the resonant networks in WPT systems.

respectively. The main advantage of this method is achieving inherent CV and CC without using any dc/dc converter in the output of the system under variable load operating conditions. Therefore, this topology can be used in a fixed coupling factor condition for a wide range of load variations, such as battery charging applications [127]–[129].

The hybrid topology and reconfigurable resonant network can also be combined to form a robust resonant network against both the misalignment and load variation [130]. The schematic of this circuit is shown in Fig. 12(c). This circuit combines the *LCC*-S and S-*LCC* topologies and supplies the load in CC or CV modes for a wide range of load and coupling factor variations.

5) Structure Comparison: The active tuning method and reconfigurable structures are attractive in terms of flexibility. However, a large number of components counts, the requirement for auxiliary circuits, and the complexity of the control techniques are the main drawbacks of these structures. As such, conventional static topologies with a higher number of resonant elements have more degrees of freedom that can be used instead of complex methods. Table V summarizes the advantages and disadvantages of the resonant topologies discussed so far.

C. Tuning and Optimization

Besides the topology selection, tuning of the resonant network plays a vital role in achieving the misalignment tolerance capability, desired power transmission efficiency, desired output features (CC or CV mode), and the ZVS operation. Fig. 13 illustrates different tuning methods that can be considered for designing a resonant network for a misalignment-tolerant IPT system. Conventionally, the resonant elements are selected to resonate at a fixed operating frequency so that the desired output features are achieved. However, there are several drawbacks to tuning the resonant network using conventional methods that are worth noting. First, the conventional methods based on parameter sweeping are time-consuming and require multiple trial and error calculations. Second, it is not guaranteed that the final solution
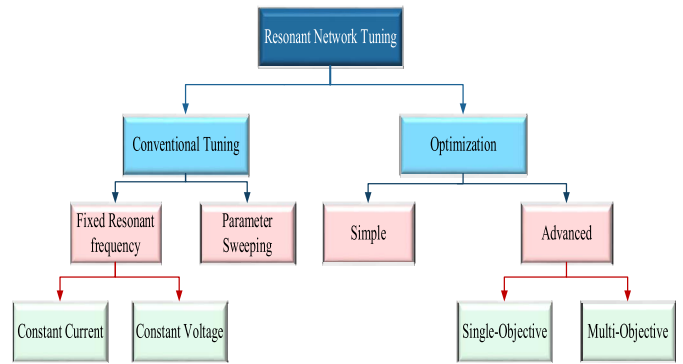
is the best possible solution. Third, the losses of the resonant network, inverter, and other elements are not considered [25]. Finally, practical constraints and objectives cannot easily be included in the conventional methods [25].

On the other hand, an optimization problem can be defined to select the resonant elements. In basic optimization methods, for example, a lossless and simplified model, combining with a single objective is considered. For instance, in [131] and [132], detuned S-S topologies are proposed, and in [101], the *LCC*-S topology is designed to offer less output power variation with respect to the coupling factor variation. However, in both studies, the losses of the system and the variation of the self-inductance of the magnetic couplers were not included. Similarly, in [133], a general T-type resonant network is analyzed, and the tuning method to achieve a misalignment-tolerant output power is presented. In [134], the resonant capacitor of a four-coil system is optimally selected to supply the load with a stable output power over a wide range of coupling coefficients. However, the losses of the system are not completely included, and it requires two additional passive repeaters.

In advanced optimization of the resonant networks, the boundaries of the system, losses, and multiple objective functions can be included. In [135], a particle swarm optimization method with the objective function of load and coupling factor independent output behavior is presented for an S-CLC-compensated IPT system. The same objective function is used in [136] for an S-SP-compensated system to achieve independent load and misalignment-tolerant features. However, in both studies, the primary-side compensation network is a series topology that suffers from unbounded current in the case of the no-load condition. In order to improve the optimization of the resonant network, the losses of the coils for an *LCC*-S topology are also included in the optimization problem, as reported in [13]. Although the output power fluctuation is reduced, the efficiency of the system was not accurately calculated due to the absence of dedicated loss modeling in the optimization. To reduce the output voltage variation to the misalignment of the coils, the sensitivity function, $(\partial V_o/\partial M)$, is defined, and the circuit is optimized [28]. This method is used to optimally design S-S, S-*LCC*, *LCC*-S, and *LCC*–*LCC* topologies to achieve low output voltage variation for a wide range of coupling factor variations. It has been shown that

TABLE VI
COMPARISON OF THE TUNING METHODS

Ref.	Topology	Optimization Method	Reported Output	Robustness Against	Core Loss Inclusion	Inverter Loss Inclusion	Coupling Factor Variation Δk [%]	Output Fluctuation ΔU [%]	Sensitivity Index β
[131]	S-S	Basic	CP	Misalignment	NO	NO	60	21	0.35
[101]	LCC-S	Basic	CP	Misalignment	NO	NO	44	7.1	0.16
[137]	S-SP	Basic	CV	Misalignment and Load	NO	NO	28.5	2.7	0.09
[135]	S-CLC	Advanced	CV	Misalignment and Load	NO	NO	50	11.7	0.23
[136]	S-SP	Advanced	CV	Misalignment and Load	NO	NO	50.8	8.9	0.18
[105]	LCC-S	Advanced	CP	Misalignment	NO	NO	37.1	8.6	0.23
[28]	S-S	Advanced	CV	Misalignment	YES	YES	43.7	21	0.48
[28]	S-LCC	Advanced	CV	Misalignment	YES	YES	43.7	6.2	0.14
[28]	LCC-S	Advanced	CV	Misalignment	YES	YES	43.7	5.2	0.11
[28]	LCC-LCC	Advanced	CV	Misalignment	YES	YES	43.7	4.5	0.10

LCC–LCC, S-*LCC*, and *LCC*-S topologies are capable of delivering CP to the load for a given coupling factor. However, other parameters, such as average efficiency, the number of components, and safe operation, should be considered for selecting a suitable resonant topology [28]. Moreover, the S-S topology has the least flexibility compared to the other *LCC*-based topologies due to its limited degree of freedom.

Table VI summarizes and compares different tuning methods from different aspects. In this table, β is a sensitivity index defined as the ratio of the output fluctuation ΔU [%] to the magnetic coupling factor variation Δk [%]. Since each reference has a different rated value, this index can be used to simplify the comparison. Lower β can be interpreted as lower output sensitivity to misalignment. According to the reported results in Table VI, it can be seen that the S-SP resonant topology has the least output voltage fluctuation. Considering the range of coupling factors, the SSP, *LCC*-S, and *LCC*–*LCC* topologies showed the best performance compared to the other topologies. However, to fairly compare these topologies, the same design conditions should be considered.

D. Comparison of the Optimized Topologies

The electrical parameters are set to be the same in order to fairly compare the misalignment tolerance capability of the various resonant topologies. Therefore, in this article, a 3.3-kW system with the specification presented in Table VII is designed according to [28]. In this comparison, all the inverter, diode bridges, resonant capacitors, and magnetic coupler losses are included based on the loss equations, which are provided in [28]. The optimization results for six different resonant topologies are shown in Fig. 14, in which the output voltage fluctuation, ΔV_o, and average efficiency, η_{ave}, of the system are calculated, and the results are presented. Since the IPT system should operate under a wide range of misalignment, the performance of the system in a wide range of coupling factors should be considered. Therefore, instead of the peak efficiency of the system, it is more beneficial to calculate and compare the average efficiencies of all topologies. In addition, the output voltage fluctuation, the number of resonant elements, and safe operation of the system under misalignment have to be taken into consideration as well.

TABLE VII
VARIABLES BOUNDARIES AND FIXED PARAMETERS

Variable/ Parameter	Description	Minimum	Maximum/ Fixed Value
L_p, L_s	Primary and secondary side self-inductance	-	270-278 µH
L_1, L_2	Resonant inductors	1 µH	500 µH
C_1, C_2, C_{s1}, C_{s2}	Resonant capacitors	1 nF	500 nF
K_n	Design set of the nominal coupling factor values	-	{0.18,0.25,0.32}
$I_p(P_{out}, k)$	Primary side coil current	0	35 A
$I_s(P_{out}, k)$	Secondary side coil current	0	35 A
ϕ	Input current phase angle	0.1	$\pi/2$
V_{dc}	DC-link voltage	-	300 V
$R_{ds(on)}$	Switch resistance	-	37 mΩ (@25°C)
r_1, r_2	Resonant inductor resistance	-	50 mΩ
r_p, r_s	LCT coil resistance	-	110 mΩ
$\tan\delta(f)$	Resonant capacitor dissipation factor	-	10^{-3}

All the high-order resonant topologies are flexible enough to supply the load with a constant output voltage. In contrast, the S-S topology shows the highest voltage variation due to the lower degree of freedom in the design. On the other hand, the *LCC*-P topology has the least average efficiency, while the S-*LCC* presented the highest efficiency and low output voltage sensitivity. The topologies of *LCC*-S and *LCC*-SP have the most tolerance with misalignment in terms of efficiency. Although these topologies do not reach peaks greater than 90% efficiency, their performance is very stable and close to
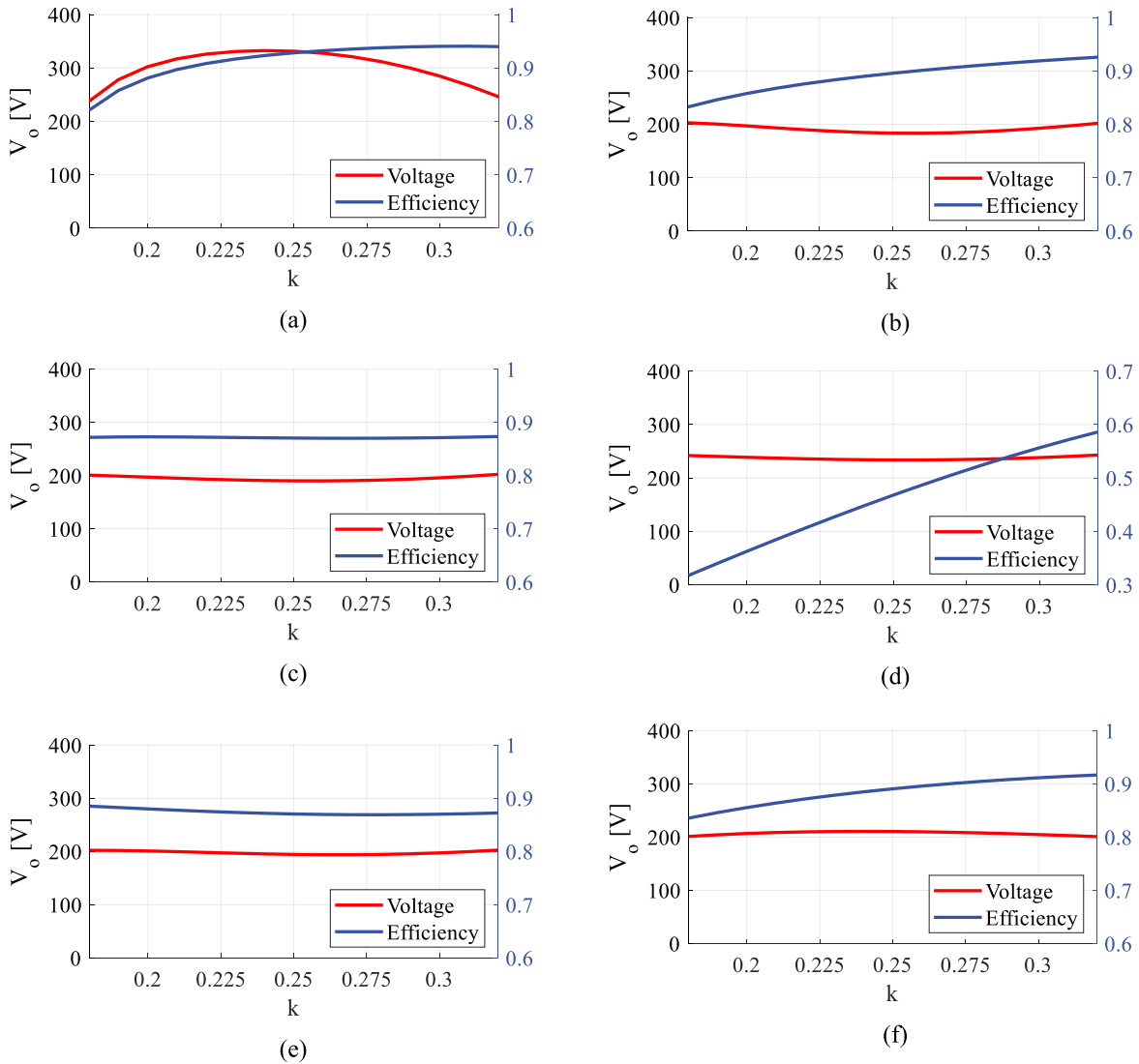
Fig. 14. Output voltage and efficiency of the optimized resonant topologies: (a) S-S: $\eta_{ave} = 91.3\%$ and $\Delta V_o = 28.5\%$, (b) S-*LCC*: $\eta_{ave} = 88.7\%$ and $\Delta V_o = 9.6\%$, (c) *LCC*-S: $\eta_{ave} = 87.1\%$ and $\Delta V_o = 6.0\%$, (d) *LCC*-P: $\eta_{ave} = 46.1\%$ and $\Delta V_o = 5.6\%$, (e) *LCC*-SP: $\eta_{ave} = 87.3\%$ and $\Delta V_o = 4.2\%$, and (f) *LCC*–*LCC*: $\eta_{ave} = 88.5\%$ and $\Delta V_o = 4.6\%$.

90% when operating under misalignment. Therefore, *LCC*-S and *LCC*-S are appropriate for systems that are assumed to operate in misalignment conditions. The other parameter that needs to be considered is the safe operation in the absence of the secondary side and at the no-load condition. From this aspect, topologies with a series compensation on the primary side, such as S-S and S-*LCC*, are not suitable for dynamic charging applications unless an appropriate protection scheme is provided on the primary side. Considering the analysis presented in Section IV-B, the *LCC*-P and *LCC*-SP topologies are not safe for operation at light load and no-load conditions due to excessive no-load voltage in the output. It can be concluded that, in terms of low output voltage variation and high average efficiency, the *LCC*-S and *LCC*–*LCC* topologies are the best candidates for dynamic charging applications. The summary of this comparison is presented in Table VIII.

V. CONTROL SYSTEMS

Power converters constitute an essential part of wireless chargers as they allow for an increment of the frequency of

TABLE VIII

MISALIGNMENT TOLERANCE COMPARISON OF THE RESONANT TOPOLOGIES

Topology	Number of Components	Average Efficiency	Voltage Variation	Safe Operation
S-S	Lowest	Best	Highest	No
S-LCC	Medium	Good	Medium	No
LCC-S	Medium	Good	Medium	Yes
LCC-P	Medium	Poor	Medium	No
LCC-SP	Highest	Good	Lowest	No
LCC-LCC	Highest	Good	Lowest	Yes

the magnetic field, and in turn, for the capacity of the system to transfer power accurately, they must be properly operated in order to achieve the expected performance without incurring excessive losses. In addition, they have to ensure the correct charging process in the battery, in which case they may be configured to provide CC, CV, or both.

The method by which the power converters operate is set by the control systems. This section will address the review of
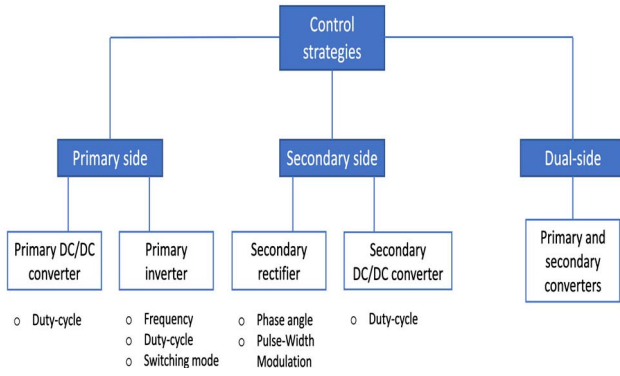
Fig. 15. Classification of control strategies for a typical wireless power transfer system.

Fig. 16. Primary-side dc-link voltage control for a wireless charging system.

the most relevant control techniques applied to cope with the misalignment in EV inductive chargers. This goal is usually set with other objectives, such as offering a CV/current/power to the load, making the system work at resonance, and reducing losses, among others. The classification of control strategies is briefly presented in Fig. 15.

As shown in Fig. 15, these control techniques can be classified into three main groups: primary-side control, secondary-side control, and dual-control. The primary-side control is executed by the power converters on the primary side, and it relies on the measurements conducted on the secondary side and computed via a wireless communication link. The secondary-side control implements the action directly on the secondary converters without wireless communication. The dual-control technique combines both primary- and secondary-side controls together.

A. Primary-Side Control

The aim of the primary-side control is to minimize the complexity, costs, and weight of the secondary side. The technique uses data sent from the secondary side to the primary side via a wireless channel. However, these wirelessly transmitted signals are subjected to delay, inaccuracy, or misleading. These parameters are especially variable in the dynamic charging where the vehicle moves during the charging process [138]. That may affect the operation of the inductive dynamic charging, which is also affected by a fast change of the misalignment of the coils. Furthermore, in real scenarios, there are multiple vehicles involved simultaneously, requiring the primary controller to deal with multiple signals at a time. This, therefore, imposes another challenge in the design of a robust and accurate dynamic charging system. As a result, wireless communication is normally avoided in EV dynamic charging. Without this communication channel, it is necessary to infer the state of the secondary side, such as the battery SoC, the CC/CV phase, or the mutual inductance. The control parameters can be estimated based on the work proposed in [139]–[142]. The primary-side control can be further divided into two main categories: the ones working on the primary dc/dc converter and those acting on the primary inverter. The primary inverter is always included in the
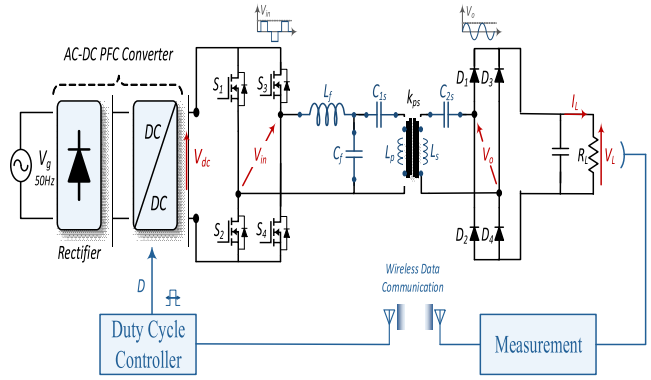
wireless charger to generate the high-frequency signal, while the use of the dc/dc converter is optional.

1) Primary DC/DC Converter: The inclusion of primary dc/dc converters in the EV wireless charger is only necessary for topologies that employ *LCL* or *LCC* compensation networks, which are foreseen as compensation networks especially suitable for operating under coil misalignment. When these compensation networks are used, the frequency is usually kept fixed by the inverter, so the control action is transferred to other parts. If the control is performed in the primary dc/dc converter, it will control the voltage in the primary inverter by regulating it to the level required by the charger. The efficiency of the power transfer is increased as the losses in the inverter are reduced. It is worth noting that, if the inverter input is set to a predefined level without proper control in transferring it to the secondary side, the resulting power produced will exceed the nominal value; as such, the battery will be overcharged, and the excess power will not be converted by the secondary dc/dc converter.

The work presented in [143] proposed a combination of proportional–derivative (PD) control and one cycle control (OCC) to generate the PWM signals required by the primary buck converter. This control technique was able to enhance the peak value of the response signal. The system dynamics were also tested under misalignment operation. The system was analyzed by varying the mutual inductance. In a similar development, Chen *et al.* [144] develop two dynamic models associated with the CC and CV charging phases. A proportional–integral (PI) control is used to adjust the duty cycle of the primary converter to different conditions of mutual inductance and charging phase while realizing zero voltage switching (ZVS). The primary dc/dc converter is sometimes enhanced to act as a power factor corrector (PFC), as shown in Fig. 16.

2) Primary Inverter: When acting on the primary inverter, three parameters can be used to adjust the system dynamics as follows.

1) *Duty Cycle:* In this technique, the inverter's output voltage is adjusted. As demonstrated in [145], varying the duty cycle of a full-bridge inverter leads to different power levels for a fixed mutual inductance. In order to cope with misalignment, those wireless chargers trying

to derive a CC/voltage/power to the load could adapt the voltage on the primary side to regulate this parameter on the secondary side. The work in [146] presents a control method in which the phase-shifting technique is applied to guarantee a safe operation of the wireless charger, even when misalignment occurs. This control algorithm ensured that the currents and the voltages on the primary side do not exceed a predefined threshold that can deteriorate or damage the system. These circumstances were identified for coil misalignment in a S-S topology. The work presented in [147] studies how to activate/deactivate the switches in a full-bridge inverter by applying a linear control for different coil alignments. The goal set is to deliver a CV to the load, even when changes in the relative position of the coils take place. However, this control strategy is only valid for a certain range of the coupling coefficient, that is, for a restricted misalignment.

2) *Frequency:* The switching frequency of the inverter is another parameter that can be tuned to guide the system to operate under some circumstances. As described previously, the secondary impedance reflected on the primary depends on the operational frequency and the mutual inductance. In order to operate with a CV/current/power on the secondary side even with misalignment, the changes in the mutual inductance can be compensated with a variation of the operational frequency. However, improper adjustment of the switching frequency can lead to bifurcation [148]. When this happens, there will be at least three frequencies with ZPA. Bifurcation could be avoided by ensuring some conditions of the quality factors of the coils. Typically, a strategy commonly referred to as "frequency perturbation and observation of the output" can seriously be affected by the bifurcation phenomenon as it moves the operating frequency according to the output measurement, just to maximize the output power. Thus, it could move from the predefined frequency to one of the bifurcation peaks [149]. On top of this issue, working on resonance for high-order compensation networks is more complex; as such, frequency adjustment is not usual in *LCL*- or *LCC*-based wireless chargers. Nevertheless, there are some frequency-control methods that are proposed in the literature. The work presented in [150] proposed a strategy in which the frequency and the phase shifting are both adjusted based on series–parallel compensation topology. The adjustment aims to achieve three goals: 1) to ensure that the required power is delivered to the battery even during misalignment conditions; 2) ensuring a nearly zero reactive input power in the interface with the grid; and 3) achieving maximum system efficiency. The work presented in [149] is based on frequency tracking for a S-S topology. In particular, the primary frequency is modified with respect to the phase between the secondary current and the output voltage of the primary inverter. A phase-locked loop (PLL) is used for the tuning in order to have a load-independent voltage gain at an acceptable efficiency, which increases
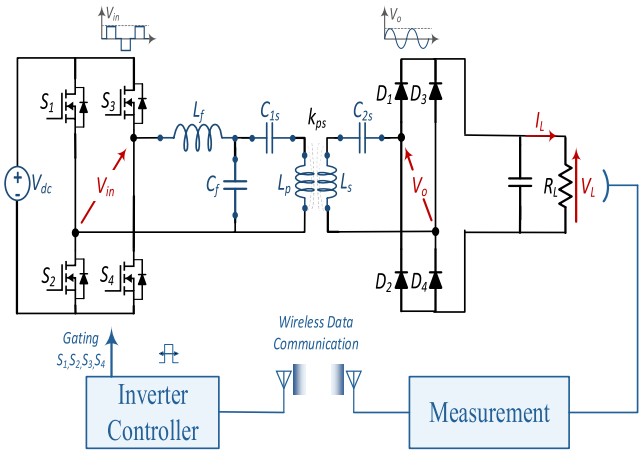

Fig. 17. Primary-side inverter control for a wireless charging system.

the complexity of the system. The proposal is evaluated for a wide range of coil misalignment, including static and dynamic conditions.

3) *Switching Mode:* By adjusting the voltage and/or current during the switching times, it is possible to make the system operate under ZVS, ZCS, or ZPA. When coil misalignment takes place, the secondary impedance reflected on the primary side changes, and in turn, the switching of the semiconductor devices should be adjusted to keep the required switching mode. In particular, ZVS is intended to reduce the system losses and EMI in the power MOSFETs. The work presented in [151] proposed a three-PID control technique for adjusting the phase shifting and the inverter frequency via a PWM signal. In contrast, ZPA tries to make the output voltage and the current of the inverter be in phase, that is, the complete input impedance (which includes the secondary impedance reflected on the primary side). In this way, the volt–ampere ratings on the components are minimized, and the reactive power stress is eliminated from the inverter [152]. Ensuring the switching mode may be performed with the tuning of the operational frequency.

In summary, Fig. 17 shows a general primary-side inverter control method designed for misalignment. The effects of the misalignment can be perceived on the primary and secondary sides. Data from the secondary side are sent to the primary side so that the inverter controller is adjusted to keep the required operation under the misalignment condition. In all these, the goal is to cope with the misalignment conditions. In addition, another objective can be set, as well as be reflected on the type of control strategy. Other compensation networks are also possible for this type of control technique. Table IX provides some key features of different methods for the EV inductive chargers.

B. Secondary-Side Control

Secondary-side control requires additional power electronic circuitries on the vehicle side, which increases the vehicle

TABLE IX
SUMMARY OF THE MAIN FEATURES OF
PRIMARY-SIDE CONTROL METHODS

Ref	Applications	Controlled variable	Controlled component	Type of control
[144]	Static	Inverter frequency and DC/DC converter duty cycle (D)	Primary DC/DC converter and inverter	CC/CV
[145]	Static	Inverter phase-shift	Primary inverter	Maximum efficiency
[146]	Static	Inverter phase-shift	Primary inverter	CP
[147]	Static/Dynamic	Inverter duty cycle (D)	Primary inverter	CV
[150]	Static	Inverter duty cycle (D) and Frequency	Primary inverter	Maximum efficiency
[149]	Static/Dynamic	Inverter frequency	Primary inverter	CP with ZPA
[151]	Static	Inverter frequency and duty cycle (D)	Primary inverter	Maximum efficiency CC

Fig. 18.   Secondary dc/dc converter control for a wireless charging system.

that regulates the inverter or a possible controlled rectifier. Moreover, it does not require the signal to be in synchronism with the primary inverter. For example, Kobayashi *et al.* [153] used an operating frequency of 10 kHz for the dc/dc converter in a system that works at 100 kHz. In a similar development, Chen *et al.* [154] used the same frequency for the converter in a system with an operating frequency of 38.4 kHz.

The dc/dc conversion can be done using different topologies. The most common ones reported in the literature are either based on boost converter, where the battery charging voltage is higher than the secondary dc bus voltage or those based on buck converter [142], [154]. The work reported in [155] is based on a boost converter due to the use of an *LCL* compensation with which they manage to reduce the nonlinear effects of the rectifier and improve the system efficiency. Both converters are adjusted by modifying the switching duty cycle, *D*. The simplest control method is using a PID controller that makes use of the error between the charging current or voltage with respect to the reference values. This type of control is capable of dealing with misalignment conditions since it constantly monitors the measurements. However, the effects of misalignment can cause the input voltage to exceed the design limits of the converter, in which case proper regulation could not be achieved. The voltage limitation in both converters can be eliminated by using a buck–boost converter, which can work in a wider range of voltages both in the secondary dc bus and the battery. This will guarantee the charging regulation against possible rises and falls of the voltage produced by the misalignments. However, the design of the converter must take into account that the output voltage is negative with respect to the input voltage. This will maximize the compatibility between different chargers and batteries. The output voltage also depends on the switching duty cycle used. The Ćuk converter and the single-ended primary-inductor converter (SEPIC) also work across the entire voltage range. The Ćuk converter features fewer ripples than the buck–boost converter [156]. On the other hand, the SEPIC converters do not have the inverse output voltage to the input voltage although they have a similar topology to the buck–boost configuration.

Apart from the traditional PID control, other control strategies are also proposed in the literature, which is tailored to

weight and the system cost. However, its technology is simpler and more robust due to the absence of communications between the primary and secondary sides. The absence of communications under misalignment is also an inconvenience for the operation of the chargers due to the high currents that can flow through the primary side. In addition, this technology also enables the development of controls with new objectives, such as maximizing charging power or its efficiency.

Secondary-side control is further classified into two types: those that act in the secondary dc/dc converter and those that operate on the secondary controlled rectifier.

1) Secondary DC/DC Converter: The use of a dc/dc converter for charging regulation is probably the simplest option available since it is based on the widely proven technology whose computational control requirements are very low. Furthermore, by connecting directly to the dc bus of the secondary, it allows the rectifier topology to be simplified to its simplest configuration, using only diodes to perform the required function. This configuration allows compatibility with different charging devices and vehicles, provided that a suitable converter and appropriate working voltages are properly chosen. In this way, the converter can work with variable input voltages to charge batteries from different manufacturers, either by applying simple constant charge strategies or other more complex ones, such as CC and CV. Fig. 18 illustrates a typical secondary dc/dc converter control method.

The control of the dc/dc converters is generally less complex since it is not necessary to act on the 85-kHz signal

pursue specific objectives not related to the charging current, voltage, or power. For example, in [157], a maximum power transfer tracking method is proposed for a buck converter. The control technique identifies the coil coupling coefficient and uses parameters, such as the operating frequency, coil resistance, charging resistance, and input voltage values to compute a value for the switching duty cycle of the converter for maximum power transfer. Since the coupling coefficient of the coils is measured in the system, the control is capable of adapting to misalignment conditions. The strategy is based on real-time coupling coefficient estimation, which is the key to achieving maximum efficiency even under misalignments. The authors estimate an efficiency improvement of 10% with their algorithm. The technique has proven to be robust as long as the system operates in resonance.

In a similar development, Kobayashi *et al.* [153] propose a maximum efficiency control on dynamic wireless charging. The strategy is based on real-time coupling coefficient estimation, which is the key to achieving maximum efficiency even under misalignments.

2) Secondary Controlled Rectifier: Controlled rectifiers are more complex converters than uncontrolled ones because they have active controlled switches that must be operated to perform the rectification function. This task is even more complex in inductive charging systems due to the synchronization between the primary inverter and the secondary controlled rectifier. The costs are also higher than when using devices that are more complex than diodes although the need to carry out regulation tasks from other elements of the system is eliminated. The control is located entirely on the secondary side and with a single-stage converter.

The advantages of controlled rectifiers over traditional diode rectifiers are [158], [159] given as follows.
1) Direct regulation of dc voltage without additional converters.
2) Lower voltage drops in the rectification process, which increases the efficiency of the system.
3) Lower losses than multistage secondary sides, as fewer elements are used.
4) Control of reactive power is possible in the ac circuit.
5) Ability to operate bidirectionally.

This single-stage topology is limited when the system must deal with misalignment. If the two-side communication is not used, the primary current's control is not achieved precisely in several compensation topologies. A voltage drop induced in the secondary may make the system unable to charge the battery since this type of converter regulates the voltage only downward except in some rarely used topologies.

There are different topologies of controlled rectifiers depending on the arrangement of the actively controlled switches. These include a single switch semiactive bridge rectifier in which one switch replaces the bottom diode used in the traditional full-bridge diode rectifier, a symmetrical bridgeless active rectifier in which each of the rectifier legs includes a diode and a switch, an asymmetrical bridgeless rectifier where one leg is composed of two switches, while the second leg contains only two diodes, and full-bridge controlled rectifier that requires four switches to operate. As an example,
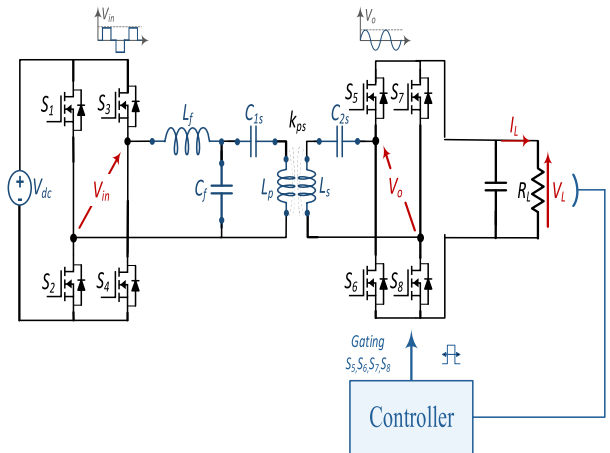

Fig. 19. Secondary side full-bridge active rectifier control for a wireless charging system.

the schematic of a full-bridge active rectifier for a wireless charging application is shown in Fig. 19.

The symmetrical bridgeless active rectifier is proposed in [160] with the main objective of controlling the charging from the secondary side with a single-stage converter. The rectifier control is based on two variables: the conduction angle β and the phase controller angle α, which indicates the period of time between the rising edge of the rectifier voltage and the falling edge of the primary resonant tank voltage. These values are obtained from the operating frequency of the system, the phase difference between voltage and current of the secondary coil, the coupling coefficient, and the equivalent impedance of the battery. The output voltage is adjusted using a PI controller. The output together with the other variables is used to operate the switches with appropriate phase shifting and delays. In this way, the system can deal with misalignments since the control signals are computed based on an estimation of the coupling factor of the coils.

Lee *et al.* [161] and Fan *et al.* [162] proposed an approach based on a symmetrical bridgeless active rectifier where the converter is operated using pulse density modulation (PDM). These proposals aim to achieve soft switching, which is compatible with the effects of misalignments. Finally, Table X summarizes the main features of different control methods on the secondary side.

C. Dual-Side Control

Control strategy considering both sides of the chargers is also possible in the EV inductive charger. Such systems are usually more complex to implement. It is because this method requires controlling two different converters simultaneously. There is also the need to communicate between both the primary and secondary sides of the charger wirelessly. Despite the higher complexity, dual-side controls provide greater flexibility and robustness. This is especially relevant against misalignments since acting on both the primary and secondary can improve efficiency and charging powers, and avoid overcurrent. The technique proposed in [163] employs a topology with a full-bridge type inverter on the primary side and a controlled

TABLE X
SUMMARY OF THE MAIN FEATURES OF SECONDARY-SIDE CONTROL

Ref	Type	Controlled variable	Controlled component	Type of control
[153]	Dynamic	Duty cycle (D)	Secondary DC/DC converter	Maximum efficiency
[157]	Static	Duty cycle (D)	Secondary DC/DC converter	Maximum power transfer
[160]	Static	Phase controller angle (α) and conduction angle (β)	Secondary rectifier	CV
[161]	Static	Pulse Density Modulation (PDM)	Secondary rectifier	CV with soft switching
[162]	Dynamic	Pulse Density Modulation (PDM)	Secondary rectifier	CV with ZVS and ZCS

TABLE XI
SUMMARY OF THE MAIN FEATURES OF DUAL-SIDE CONTROL

Ref	Type	Controlled variable	Controlled component	Type of control
[163]	Static	Primary and Secondary Pulse Width (α β)	Primary Inverter and Secondary Rectifier	CC-CV
[164]	Static	Primary inverter phase-shift and secondary hysteresis control	Primary inverter and secondary charging protection circuit	CC-CV
[165]	Static	Primary Voltage, Charging Voltage and Efficiency	Primary and Secondary DC/DC converters	Maximum efficiency
[166]	Static	Primary Voltage, Charging Voltage and Efficiency	Primary and Secondary DC/DC converters	Maximum efficiency
[167]	Static	Primary Voltage, Charging Voltage and Efficiency	Primary and Secondary DC/DC converters	Maximum efficiency
[60]	Static	Primary Voltage, Charging Voltage and Efficiency	Primary Inverter and Secondary Rectifier	Maximum efficiency
[55]	Static	PFC duty cycle, inverter mode switching, rectifier duty cycle and phase angle	Primary PFC, Primary Inverter and Secondary Rectifier	Maximum efficiency
[56]	Static	Efficiency	Primary Inverter and Secondary Rectifier	Maximum efficiency CC/CV with ZVS

rectifier with a dual-active-bridge converter configuration on the secondary side for optimizing the efficiency under the large variation of both coupling coefficient and load.

The requirement to communicate between both sides of the charger is not always necessary, as demonstrated in [164]. However, this is still a robust solution where the primary controller act on the primary side, and the secondary controller ensures that the charging process follows the CC/CV curve. The primary control is carried out following the phase-shifting technique, where the load is regulated by the secondary controller. The main advantage of this system is that, without establishing communication between both sides of the charger, the primary current does not exceed the maximum value. This is a key factor for dealing with misalignment since the increase in the primary-side current is one of the problems caused by this contingency.

Li *et al.* [165] propose a buck converter and a high-frequency half-bridge inverter on the primary side, while a passive half-wave rectifier with a boost converter is employed on the secondary side. The objective is to regulate the load by controlling each of the converters simultaneously so that the IPT system can work at the maximum efficiency point even under the large variation of load and misalignment. This control strategy is based on three fundamental aspects: 1) to set the working frequency required to operate the secondary side in resonance; 2) use the buck converter to regulate the input voltage and, thus, compensate for the voltage increase that occurs in the secondary side in the event of misalignments with the SS topology; and 3) to vary the value of the equivalent resistance of the battery using the boost converter in the secondary side. It is obvious that the working frequency is fixed and does not influence the control; however, both the input voltage and the equivalent resistance of the battery can be adjusted to control the battery charging voltage. The challenge here lies in how to operate these points since there is a constant load voltage curve that relates different levels of input voltage and equivalent resistance. This curve operates in real time, which ensures the goal of maximum efficiency even with dynamic misalignments. According to the authors, the

overall efficiency of the system under misalignment improves by more than 10% with gaps of 25 cm with the proposed algorithm. The work presented in [166] proposed an algorithm that achieves maximum efficiency by calculating the CV curve. An improved version of this control strategy is proposed in [167], which takes into account the possible variations in mutual inductance when the misalignment between both coils is modified. The control technique is based on estimating the coupling factor by detecting the variations in the load resistance or the output voltage and using these data to adjust the duty cycle of the converters. Adjusting the buck–boost converter with the proposed controller achieves improvements of up to 20% in system efficiency.

Other control techniques reported in the literature were applied to other converter topologies. For example, Li *et al.* [168] proposed a pulse density modulated (PDM) full-bridge converter topology for the primary inverter, which combines the advantages of PDM and ZVS techniques. Despite its similarity to the traditional full-bridge inverter, this topology incorporates a ZVS branch connected between both output terminals of the converter to ensure soft switching with ZVS current. An active rectifier using the same PDM technique is utilized on the secondary side. The combined operation of both converters eliminates the need to use a dc/dc converter on the secondary side of the charger; this

makes it possible to reduce the conversion losses and the components used. This goal is achieved by operating the converters following a maximum efficiency point tracking technique. The authors have verified the effectiveness of this technique when different coupling factors. The work reported in [169] proposed a topology whose main contribution is the introduction of a switching voltage regulator, which autonomously regulates the charger output voltage to ensure a constant output value even with misalignment. In [170], the optimal load impedance is achieved by adjusting the inverter output voltage under a dual-sided control strategy. The active rectifier control is based on a phase-locked method for the output current/voltage. Chen *et al.* [107] proposed a strategy for semi-impedance matching under large load variations conditions. The strategy is based on properly selecting full- and half-bridge modes of the inverter and the rectifier. Finally, some key features of the dual-sided control are provided in Table XI.

D. Discussion

Control in wireless chargers is usually implemented to regulate the charging power in the battery in a CC/CV mode.

To proceed with this regulation correctly, efficiency or misalignment effects should be considered. The effectiveness of the control strategy depends on the power converter, where it is applied and the data provided by the communication system. Table XII compares the pros and cons of applying the control to each power converter.

VI. Challenges and Future Developments

The IPT technology has huge potential to decrease the reliance on fossil fuels and minimize the greenhouse gases emissions by accelerating the penetrations of EVs. However, the misalignment issues prevent the high penetration of this technology. Different methods have been proposed so far to address the issues; however, they all have some common challenges as follows.

1) New methods increase the cost of the IPT system, especially for dynamic wireless charging. It is considered that the higher cost can be acceptable from the gain of battery size reduction and the user's convenience.
2) More complexity in design and control. It is obvious that adding more windings into the coupler pad or applying a new control method will increase the complexity of the system. It is better to consider this downside and accept the fact that not every method can be utilized in real scenarios.
3) Communication between the source and vehicle sides can be delayed in the real scenario, especially for dynamic charging. This challenge affects the accuracy of the real-time control system in the IPT system. One solution for this matter is to perform independent control on each side to reduce the communication requirement between the two sides.
4) The safety concern of electric and magnetic fields (EMFs) from the IPT charging on humans. This is a common issue in the IPT system, especially under high misalignment conditions. The EMF shielding is always required to guarantee that the EMF level is kept below a certain value [20].
5) Interoperability between different charging systems must be guaranteed to facilitate the integration of this technology. Control systems can alleviate part of this problem. However, necessary regulation should play a more important role in this task. The SAE J2954 standard classifies charger types based on the gap between the two coils to ensure compatibility. Similarly, this standard also establishes minimum efficiency values for the maximum X, Y, Z, and rotational offsets.
6) The integration of the transmitting coils for dynamic charging is quite a challenge. In addition to the requirement to establish a reliable communication system, as mentioned above, misalignment is more serious than static charging. First, wireless chargers face different types of roads, as their topology affects the depth at which the coils are located [171]. Horizontal misalignment also affects the efficiency of the process, so autonomous coil alignment systems will be necessary to minimize misalignment [172].

Based on the extensive review in this article combined with the ongoing research, the authors suggest the possibility of further studies regarding the misalignment issues in EV wireless charging. For static operations, we outline the following topics.

1) Development of sensor systems for aiding the vehicle alignment to avoid misalignment physically. The system could be incorporated into a visual interface such that the driver can place the vehicle in the most convenient position. Autonomous vehicles can benefit from this kind of system.
2) Most coupler designs aim at developing robust structures with a low variation on their coupling coefficients. However, the variation is inevitable for realistic misalignment conditions; therefore, the compensation networks can be adjusted to keep the system's efficiency at an acceptable level. Potential future works should integrate compensation networks and couplers so that the variations of both parts could be effectively canceled out altogether.
3) The introduction of electromagnetic metamaterials on the IPT system for improving efficiency under the conditions of lateral misalignment and angular offset. Theoretically, metamaterials can help in the increment of the self-inductance and the mutual inductance compared to the ferrite core.
4) Improvement of communication data of the coupling factor between primary and secondary sides for better accuracy, security, and reduced delay time in tuning the components.
5) Inclusion of artificial intelligence techniques to detect if the changes in the coupling coefficient is due to coil misalignment or to the presence of an intermediate object, as these two conditions are handled in different ways.

TABLE XII
SUMMARY OF THE MAIN FEATURES OF THE CONTROL STRATEGIES

Type of control	Converter	Pros	Cons
Primary side	DC/DC converter	• Operating frequency is different from the inductive link. • Improvement of the efficiency of the grid rectifiers when operating as PFC.	• Requires a communication system to control misalignment. • It cannot implement maximum efficiency strategies.
	Inverter	• Easy output voltage control. • No need to use a DC/DC converter. • Ability to adjust the frequency to improve resonance.	• Requires communication to control misalignment. • Phase-shifting can derive in hard switching. • It cannot implement maximum efficiency strategies.
Secondary side	DC/DC converter	• No communications are needed for simple charging control, even with misalignment. • Operating frequency is different from inductive link.	• Impossibility of simultaneously controlling the charging power and the efficiency.
	Controlled rectifier	• No communications are needed for simple charging control, even with misalignment. • No need to use a DC/DC converter.	• It requires synchronization between the controller and the AC signal.
Dual side		• It can provide better maximum efficiency strategies. • It is able to keep charging power under misalignment without exceeding component limits.	• Communications are required in most strategies.

Misalignment is intrinsic in dynamic charging; therefore, the charger must adapt quickly to the changes in the mutual inductance. The future topics mentioned for stationary charging can be partly applied for dynamic systems. Besides that, some future topics can be addressed for this kind of application.

1) More investigation of power converters to work as a configurable compensation structure. This is expended from Sections IV-C and IV-D in this article. Prediction models may be useful to determine the proper configuration of the switches of the power converters so that the reactance provided by the converters can be tuned fast.

2) Power converters (specifically primary inverter and secondary rectifier) must adapt their operation to provide the power required by an operational point with a specific value of mutual inductance. New strategies about how to modify the operational point of the power converters could be analyzed so that the losses and the stresses of the components are reduced during these variations. Model predictive control (MPC) may be suitable for this purpose.

3) Combining control of power converters and active turning of compensation networks simultaneously to an efficient reconfiguration of the complete system to guarantee a minimum performance level. Restricting the magnetic field is also a requirement that must be met in dynamic chargers. Active shielding techniques may also be the solution to achieve this goal with frequent changes. In this sense, predictive algorithms could be used to configure them and adapt them to the continued variations of the magnetic field.

VII. CONCLUSION

This article gives a comprehensive review of the EVs' inductive charging system focusing on how to address the misalignment issues within the wireless charging process. Unlike the conventional conductive charger, the relative position between the transmitter and the receiver changes frequently in the inductive charger resulting in a reduction in the power transfer and efficiency. Various techniques have been proposed regarding the magnetic coupler topologies, compensation techniques, and control strategies, aiming to improve the system tolerance against misalignment. Detailed presentations are given that summarize, analyze, and compare these methods to identify their advantages and disadvantages. Based on the provided findings in this work, the authors' recommendations for further research on wireless EV chargers regarding

coils misalignments are: 1) improvement of vehicle alignment through the deployment of sensor systems; 2) design of active compensation networks and couplers systems for misalignment effect mitigation; 3) use of electromagnetic metamaterial to compensate for lateral misalignment and angular offset; 4) improvement of primary-secondary systems communication to increase efficiency; 5) use of artificial intelligence for detection of coil misalignment versus the presence of an intermediate object; 6) study of power converters as compensation devices; 7) new control strategies for misalignment compensation; and 8) combination of power converter controls and active tuning of compensation networks to increase efficiency. With continuous technology development, the IPT system will become more and more stable with misalignment, which will accelerate the penetration of EV wireless charging in the near term.

REFERENCES

[1] G. A. Covic and J. T. Boys, "Inductive power transfer," *Proc. IEEE*, vol. 101, no. 6, pp. 1276–1289, Jun. 2013, doi: 10.1109/JPROC.2013.2244536.

[2] Z. Zhang, H. Pang, A. Georgiadis, and C. Cecati, "Wireless power transfer—An overview," *IEEE Trans. Ind. Electron.*, vol. 66, no. 2, pp. 1044–1058, Feb. 2019, doi: 10.1109/TIE.2018.2835378.

[3] A. Ahmad, M. S. Alam, and R. Chabaan, "A comprehensive review of wireless charging technologies for electric vehicles," *IEEE Trans. Transport. Electrific.*, vol. 4, no. 1, pp. 38–63, Mar. 2018, doi: 10.1109/TTE.2017.2771619.

[4] G. A. Covic and J. T. Boys, "Modern trends in inductive power transfer for transportation applications," *IEEE J. Emerg. Sel. Topics Power Electron.*, vol. 1, no. 1, pp. 28–41, Mar. 2013, doi: 10.1109/JESTPE.2013.2264473.

[5] S. Li and C. C. Mi, "Wireless power transfer for electric vehicle applications," *IEEE J. Emerg. Sel. Topics Power Electron.*, vol. 3, no. 1, pp. 4–17, Mar. 2015, doi: 10.1109/JESTPE.2014.2319453.

[6] D. Patil, M. K. McDonough, J. M. Miller, B. Fahimi, and P. T. Balsara, "Wireless power transfer for vehicular applications: Overview and challenges," *IEEE Trans. Transport. Electrific.*, vol. 4, no. 1, pp. 3–37, Mar. 2018, doi: 10.1109/TTE.2017.2780627.

[7] A. Triviño, J. M. González-González, and J. A. Aguado, "Wireless power transfer technologies applied to electric vehicles: A review," *Energies*, vol. 14, no. 6, p. 1547, Mar. 2021, doi: 10.3390/en14061547.

[8] X. Mou, D. T. Gladwin, R. Zhao, and H. Sun, "Survey on magnetic resonant coupling wireless power transfer technology for electric vehicle charging," *IET Power Electron.*, vol. 12, no. 12, pp. 3005–3020, 2019, doi: 10.1049/iet-pel.2019.0529.

[9] S. Y. Choi, B. W. Gu, S. Y. Jeong, and C. T. Rim, "Advances in wireless power transfer systems for roadway-powered electric vehicles," *IEEE J. Emerg. Sel. Topics Power Electron.*, vol. 3, no. 1, pp. 18–36, Mar. 2015, doi: 10.1109/JESTPE.2014.2343674.

[10] C. C. Mi, G. Buja, S. Y. Choi, and C. T. Rim, "Modern advances in wireless power transfer systems for roadway powered electric vehicles," *IEEE Trans. Ind. Electron.*, vol. 63, no. 10, pp. 6533–6545, Oct. 2016, doi: 10.1109/TIE.2016.2574993.

[11] A. C. Bagchi, A. Kamineni, R. A. Zane, and R. Carlson, "Review and comparative analysis of topologies and control methods in dynamic wireless charging of electric vehicles," *IEEE J. Emerg. Sel. Topics Power Electron.*, vol. 9, no. 4, pp. 4947–4962, Aug. 2021, doi: 10.1109/JESTPE.2021.3058968.

[12] J. Dai and D. C. Ludois, "A survey of wireless power transfer and a critical comparison of inductive and capacitive coupling for small gap applications," *IEEE Trans. Power Electron.*, vol. 30, no. 11, pp. 6017–6029, Nov. 2015, doi: 10.1109/TPEL.2015.2415253.

[13] S. Y. R. Hui, W. Zhong, and C. K. Lee, "A critical review of recent progress in mid-range wireless power transfer," *IEEE Trans. Power Electron.*, vol. 29, no. 9, pp. 4500–4511, Sep. 2014, doi: 10.1109/TPEL.2013.2249670.

[14] W. Zhang and C. C. Mi, "Compensation topologies of high-power wireless power transfer systems," *IEEE Trans. Veh. Technol.*, vol. 65, no. 6, pp. 4768–4778, Jul. 2016, doi: 10.1109/TVT.2015.2454292.

[15] C. Jiang, K. T. Chau, C. Liu, and C. H. T. Lee, "An overview of resonant circuits for wireless power transfer," *Energies*, vol. 10, no. 7, pp. 894-1–894-20, Jun. 2017, doi: 10.3390/en10070894.

[16] A. A. S. Mohamed, A. A. Shaier, H. Metwally, and S. I. Selem, "A comprehensive overview of inductive pad in electric vehicles stationary charging," *Appl. Energy*, vol. 262, Mar. 2020, Art. no. 114584, doi: 10.1016/j.apenergy.2020.114584.

[17] C. Rong *et al.*, "A critical review of metamaterial in wireless power transfer system," *IET Power Electron.*, pp. 1541–1559, May 2021, doi: 10.1049/pel2.12099.

[18] W. Lee and Y.-K. Yoon, "Wireless power transfer systems using metamaterials: A review," *IEEE Access*, vol. 8, pp. 147930–147947, 2020, doi: 10.1109/ACCESS.2020.3015176.

[19] Y. Zhang, Z. Yan, J. Zhu, S. Li, and C. Mi, "A review of foreign object detection (FOD) for inductive power transfer systems," *eTransportation*, vol. 1, Aug. 2019, Art. no. 100002, doi: 10.1016/j.etran.2019.04.002.

[20] *Wireless Power Transfer for Light-Duty Plug-in/Electric Vehicles and Alignment Methodology*, document SAE J2954, SAE International, Oct. 2020.

[21] A. A. S. Mohamed, S. An, and O. Mohammed, "Coil design optimization of power pad in IPT system for electric vehicle applications," *IEEE Trans. Magn.*, vol. 54, no. 4, pp. 1–5, Apr. 2018, doi: 10.1109/TMAG.2017.2784381.

[22] M. Budhia, G. A. Covic, and J. T. Boys, "Design and optimization of circular magnetic structures for lumped inductive power transfer systems," *IEEE Trans. Power Electron.*, vol. 26, no. 11, pp. 3096–3108, Nov. 2011, doi: 10.1109/TPEL.2011.2143730.

[23] M. Budhia, G. Covic, and J. Boys, "A new IPT magnetic coupler for electric vehicle charging systems," in *Proc. IECON 36th Annu. Conf. IEEE Ind. Electron. Soc.*, Nov. 2010, pp. 2487–2492, doi: 10.1109/IECON.2010.5675350.

[24] H. Kim, C. Song, J. Kim, J. Kim, and J. Kim, "Shielded coil structure suppressing leakage magnetic field from 100W-class wireless power transfer system with higher efficiency," in *IEEE MTT-S Int. Microw. Symp. Dig.*, May 2012, pp. 6–83, doi: 10.1109/IMWS.2012.6215825.

[25] A. Ramezani, S. Farhangi, H. Iman-Eini, B. Farhangi, R. Rahimi, and G. R. Moradi, "Optimized LCC-series compensated resonant network for stationary wireless EV chargers," *IEEE Trans. Ind. Electron.*, vol. 66, no. 4, pp. 2756–2765, Apr. 2019, doi: 10.1109/TIE.2018.2840502.

[26] X. Wang, J. Xu, M. Mao, and H. Ma, "An LCL-based SS compensated WPT converter with wide ZVS range and integrated coil structure," *IEEE Trans. Ind. Electron.*, vol. 68, no. 6, pp. 4882–4893, Jun. 2021, doi: 10.1109/TIE.2020.2989707.

[27] R. Bosshard, J. W. Kolar, J. Mühlethaler, I. Stevanović, B. Wunsch, and F. Canales, "Modeling and η-α-Pareto optimization of inductive power transfer coils for electric vehicles," *IEEE J. Emerg. Sel. Topics Power Electron.*, vol. 3, no. 1, pp. 50–64, Mar. 2015, doi: 10.1109/JESTPE.2014.2311302.

[28] A. Ramezani and M. Narimani, "Optimized electric vehicle wireless chargers with reduced output voltage sensitivity to misalignment," *IEEE J. Emerg. Sel. Topics Power Electron.*, vol. 8, no. 4, pp. 3569–3581, Dec. 2020, doi: 10.1109/JESTPE.2019.2958932.

[29] S. Bandyopadhyay, P. Venugopal, J. Dong, and P. Bauer, "Comparison of magnetic couplers for IPT-based EV charging using multiobjective optimization," *IEEE Trans. Veh. Technol.*, vol. 68, no. 6, pp. 5416–5429, Jun. 2019, doi: 10.1109/TVT.2019.2909566.

[30] Z. Fang, T. Cai, S. Duan, and C. Chen, "Optimal design methodology for LLC resonant converter in battery charging applications based on time-weighted average efficiency," *IEEE Trans. Power Electron.*, vol. 30, no. 10, pp. 5469–5483, Oct. 2015, doi: 10.1109/TPEL.2014.2379278.

[31] M. K. Kazimierczuk and D. Czarkowski, *Resonant Power Converters*. Hoboken, NJ, USA: Wiley, 2012.

[32] K. Kadem, M. Bensetti, Y. L. Bihan, E. Labouré, and M. Debbou, "Optimal coupler topology for dynamic wireless power transfer for electric vehicle," *Energies*, vol. 14, no. 13, p. 3983, Jul. 2021, doi: 10.3390/en14133983.

[33] S. Wang and D. G. Dorrell, "Copper loss analysis of EV charging coupler," *IEEE Trans. Magn.*, vol. 51, no. 11, pp. 1–4, Nov. 2015, doi: 10.1109/TMAG.2015.2445097.

[34] C. R. Sullivan, "Cost-constrained selection of strand diameter and number in a Litz-wire transformer winding," *IEEE Trans. Power Electron.*, vol. 16, no. 2, pp. 281–288, Mar. 2001, doi: 10.1109/63.911153.

[35] P. L. Dowell, "Effects of eddy currents in transformer windings," *Proc. Inst. Electr. Eng.*, vol. 113, no. 8, pp. 1387–1394, Aug. 1966, doi: 10.1049/piee.1966.0236.

[36] R. P. Wojda and M. K. Kazimierczuk, "Winding resistance of Litz-wire and multi-strand inductors," *IET Power Electron.*, vol. 5, no. 2, pp. 257–268, Feb. 2012, doi: 10.1049/IET-PEL.2010.0359.

[37] C. R. Sullivan, "Optimal choice for number of strands in a Litz-wire transformer winding," *IEEE Trans. Power Electron.*, vol. 14, no. 2, pp. 283–291, Mar. 1999, doi: 10.1109/63.750181.

[38] A. Reatti and M. K. Kazimierczuk, "Comparison of various methods for calculating the AC resistance of inductors," *IEEE Trans. Magn.*, vol. 38, no. 3, pp. 1512–1518, May 2002, doi: 10.1109/20.999124.

[39] M. Lu and K. D. T. Ngo, "Analytical calculation of proximity-effect resistance for planar coil with Litz wire and ferrite plate in inductive power transfer," *IEEE Trans. Ind. Appl.*, vol. 55, no. 3, pp. 2984–2991, May 2019, doi: 10.1109/TIA.2018.2890366.

[40] Z. Pantic and S. Lukic, "Computationally-efficient, generalized expressions for the proximity-effect in multi-layer, multi-turn tubular coils for wireless power transfer systems," *IEEE Trans. Magn.*, vol. 49, no. 11, pp. 5404–5416, Nov. 2013, doi: 10.1109/TMAG.2013.2264486.

[41] A. Roßkopf, E. Bär, C. Joffe, and C. Bonse, "Calculation of power losses in Litz wire systems by coupling FEM and PEEC method," *IEEE Trans. Power Electron.*, vol. 31, no. 9, pp. 6442–6449, Sep. 2016, doi: 10.1109/TPEL.2015.2499793.

[42] Q. Deng *et al.*, "Frequency-dependent resistance of Litz-wire square solenoid coils and quality factor optimization for wireless power transfer," *IEEE Trans. Ind. Electron.*, vol. 63, no. 5, pp. 2825–2837, May 2016, doi: 10.1109/TIE.2016.2518126.

[43] M. Mohammad, S. Choi, Z. Islam, S. Kwak, and J. Baek, "Core design and optimization for better misalignment tolerance and higher range of wireless charging of PHEV," *IEEE Trans. Transport. Electrific.*, vol. 3, no. 2, pp. 445–453, Jun. 2017, doi: 10.1109/TTE.2017.2663662.

[44] J. M. Miller and A. Daga, "Elements of wireless power transfer essential to high power charging of heavy duty vehicles," *IEEE Trans. Transport. Electrific.*, vol. 1, no. 1, pp. 26–39, Jun. 2015, doi: 10.1109/TTE.2015.2426500.

[45] Y. Nagatsuka, N. Ehara, Y. Kaneko, S. Abe, and T. Yasuda, "Compact contactless power transfer system for electric vehicles," in *Proc. Int. Power Electron. Conf. (ECCE ASIA)*, Jun. 2010, pp. 807–813, doi: 10.1109/IPEC.2010.5543313.

[46] M. Budhia, J. T. Boys, G. A. Covic, and C.-Y. Huang, "Development of a single-sided flux magnetic coupler for electric vehicle IPT charging systems," *IEEE Trans. Ind. Electron.*, vol. 60, no. 1, pp. 318–328, Jan. 2013, doi: 10.1109/TIE.2011.2179274.

[47] M. G. S. Pearce, G. A. Covic, and J. T. Boys, "Robust ferrite-less double D topology for roadway IPT applications," *IEEE Trans. Power Electron.*, vol. 34, no. 7, pp. 6062–6075, Jul. 2019, doi: 10.1109/TPEL.2018.2883129.

[48] K. Song *et al.*, "Design of DD coil with high misalignment tolerance and low EMF emissions for wireless electric vehicle charging systems," *IEEE Trans. Power Electron.*, vol. 35, no. 9, pp. 9034–9045, Sep. 2020, doi: 10.1109/TPEL.2020.2971967.

[49] Z. Luo, X. Wei, M. G. S. Pearce, and G. A. Covic, "Multiobjective optimization of inductive power transfer double-D pads for electric vehicles," *IEEE Trans. Power Electron.*, vol. 36, no. 5, pp. 5135–5146, May 2021, doi: 10.1109/TPEL.2020.3029789.

[50] M. Mohammad, S. Choi, and M. E. Elbuluk, "Loss minimization design of ferrite core in a DD-coil-based high-power wireless charging system for electrical vehicle application," *IEEE Trans. Transport. Electrific.*, vol. 5, no. 4, pp. 957–967, Dec. 2019, doi: 10.1109/TTE.2019.2940878.

[51] J. M. Miller *et al.*, "Demonstrating dynamic wireless charging of an electric vehicle: The benefit of electrochemical capacitor smoothing," *IEEE Power Electron. Mag.*, vol. 1, no. 1, pp. 12–24, Mar. 2014, doi: 10.1109/MPEL.2014.2300978.

[52] L. Xiang, Y. Sun, C. Tang, X. Dai, and C. Jiang, "Design of crossed DD coil for dynamic wireless charging of electric vehicles," in *Proc. IEEE PELS Workshop Emerg. Technol., Wireless Power Transf. (WoW)*, May 2017, pp. 1–5, doi: 10.1109/WoW.2017.7959422.

[53] M. G. S. Pearce, G. A. Covic, and J. T. Boys, "Reduced ferrite double D pad for roadway IPT applications," *IEEE Trans. Power Electron.*, vol. 36, no. 5, pp. 5055–5068, May 2021, doi: 10.1109/TPEL.2020.3032691.

[54] J. Shin *et al.*, "Design and implementation of shaped magnetic-resonance-based wireless power transfer system for roadway-powered moving electric vehicles," *IEEE Trans. Ind. Electron.*, vol. 61, no. 3, pp. 1179–1192, Mar. 2014, doi: 10.1109/TIE.2013.2258294.

[55] B.-M. Song, R. Kratz, and S. Gurol, "Contactless inductive power pickup system for Maglev applications," in *Proc. IEEE Ind. Appl. Conf. 37th IAS Annu. Meeting*, vol. 3, Oct. 2002, pp. 1586–1591, doi: 10.1109/IAS.2002.1043746.

[56] W. Y. Lee *et al.*, "Finite-width magnetic mirror models of mono and dual coils for wireless electric vehicles," *IEEE Trans. Power Electron.*, vol. 28, no. 3, pp. 1413–1428, Mar. 2013, doi: 10.1109/TPEL.2012.2206404.

[57] J. Huh, S. W. Lee, W. Y. Lee, G. H. Cho, and C. T. Rim, "Narrow-width inductive power transfer system for online electrical vehicles," *IEEE Trans. Power Electron.*, vol. 26, no. 12, pp. 3666–3679, Dec. 2011, doi: 10.1109/TPEL.2011.2160972.

[58] S. Y. Choi, S. Y. Jeong, B. W. Gu, G. C. Lim, and C. T. Rim, "Ultraslim S-type power supply rails for roadway-powered electric vehicles," *IEEE Trans. Power Electron.*, vol. 30, no. 11, pp. 6456–6468, Nov. 2015, doi: 10.1109/TPEL.2015.2444894.

[59] Z. Wang *et al.*, "A novel magnetic coupling mechanism for dynamic wireless charging system for electric vehicles," *IEEE Trans. Veh. Technol.*, vol. 67, no. 1, pp. 124–133, Jan. 2018, doi: 10.1109/TVT.2017.2776348.

[60] G. R. Nagendra, G. A. Covic, and J. T. Boys, "Sizing of inductive power pads for dynamic charging of EVs on IPT highways," *IEEE Trans. Transport. Electrific.*, vol. 3, no. 2, pp. 405–417, Jun. 2017, doi: 10.1109/TTE.2017.2666554.

[61] V.-B. Vu, M. Dahidah, V. Pickert, and V.-T. Phan, "A high-power multiphase wireless dynamic charging system with low output power pulsation for electric vehicles," *IEEE J. Emerg. Sel. Topics Power Electron.*, vol. 8, no. 4, pp. 3592–3608, Dec. 2020, doi: 10.1109/JESTPE.2019.2932302.

[62] J. Pries, V. P. N. Galigekere, O. C. Onar, and G.-J. Su, "A 50-kW three-phase wireless power transfer system using bipolar windings and series resonant networks for rotating magnetic fields," *IEEE Trans. Power Electron.*, vol. 35, no. 5, pp. 4500–4517, May 2020, doi: 10.1109/TPEL.2019.2942065.

[63] S. Cui, Z. Wang, S. Han, and C. Zhu, "Analysis and design of multiphase receiver with reduction of output fluctuation for EV dynamic wireless charging system," *IEEE Trans. Power Electron.*, vol. 34, no. 5, pp. 4112–4124, May 2019, doi: 10.1109/TPEL.2018.2859368.

[64] A. Zaheer, M. Budhia, D. Kacprzak, and G. A. Covic, "Magnetic design of a 300 w under-floor contactless power transfer system," in *Proc. IECON 37th Annu. Conf. IEEE Ind. Electron. Soc.*, Nov. 2011, pp. 1408–1413, doi: 10.1109/IECON.2011.6119514.

[65] A. Zaheer, G. A. Covic, and D. Kacprzak, "A bipolar pad in a 10-kHz 300-W distributed IPT system for AGV applications," *IEEE Trans. Ind. Electron.*, vol. 61, no. 7, pp. 3288–3301, Jul. 2014, doi: 10.1109/TIE.2013.2281167.

[66] S. Kim, G. A. Covic, and J. T. Boys, "Tripolar pad for inductive power transfer systems for EV charging," *IEEE Trans. Power Electron.*, vol. 32, no. 7, pp. 5045–5057, Jul. 2017, doi: 10.1109/TPEL.2016.2606893.

[67] S. Kim, G. A. Covic, and J. T. Boys, "Comparison of tripolar and circular pads for IPT charging systems," *IEEE Trans. Power Electron.*, vol. 33, no. 7, pp. 6093–6103, Jul. 2018, doi: 10.1109/TPEL.2017.2740044.

[68] C. Park, S. Lee, S. Y. Jeong, G. H. Cho, and C. T. Rim, "Uniform power I-type inductive power transfer system with DQ-power supply rails for on-line electric vehicles," *IEEE Trans. Power Electron.*, vol. 30, no. 11, pp. 6446–6455, Nov. 2015, doi: 10.1109/TPEL.2015.2420372.

[69] A. Zaheer, H. Hao, G. A. Covic, and D. Kacprzak, "Investigation of multiple decoupled coil primary pad topologies in lumped IPT systems for interoperable electric vehicle charging," *IEEE Trans. Power Electron.*, vol. 30, no. 4, pp. 1937–1955, Apr. 2015, doi: 10.1109/TPEL.2014.2329693.

[70] G. A. Covic, J. T. Boys, M. L. G. Kissin, and H. G. Lu, "A three-phase inductive power transfer system for roadway-powered vehicles," *IEEE Trans. Ind. Electron.*, vol. 54, no. 6, pp. 3370–3378, Dec. 2007, doi: 10.1109/TIE.2007.904025.

[71] G. Elliott, S. Raabe, G. A. Covic, and J. T. Boys, "Multiphase pickups for large lateral tolerance contactless power-transfer systems," *IEEE Trans. Ind. Electron.*, vol. 57, no. 5, pp. 1590–1598, May 2010, doi: 10.1109/TIE.2009.2031184.

[72] B. Song, S. Cui, Y. Li, and C. Zhu, "A narrow-rail three-phase magnetic coupler with uniform output power for EV dynamic wireless charging," *IEEE Trans. Ind. Electron.*, vol. 68, no. 8, pp. 6456–6469, Aug. 2021, doi: 10.1109/TIE.2020.3005072.

[73] U. Iruretagoyena, I. Villar, A. Garcia-Bediaga, L. Mir, and H. Camblong, "Design and characterization of a meander-type dynamic inductively coupled power transfer coil," *IEEE Trans. Ind. Appl.*, vol. 53, no. 4, pp. 3950–3959, Jul. 2017, doi: 10.1109/TIA.2017. 2692199.

[74] M. Kim, H. Kim, D. Kim, Y. Jeong, H.-H. Park, and S. Ahn, "A three-phase wireless-power-transfer system for online electric vehicles with reduction of leakage magnetic fields," *IEEE Trans. Microw. Theory Techn.*, vol. 63, no. 11, pp. 3806–3813, Nov. 2015, doi: 10.1109/TMTT.2015.2479627.

[75] S. Raabe and G. A. Covic, "Practical design considerations for contactless power transfer quadrature pick-ups," *IEEE Trans. Ind. Electron.*, vol. 60, no. 1, pp. 400–409, Aug. 2013, doi: 10.1109/ TIE.2011.2165461.

[76] J. H. Kim *et al.*, "Development of 1-MW inductive power transfer system for a high-speed train," *IEEE Trans. Ind. Electron.*, vol. 62, no. 10, pp. 6242–6250, Oct. 2015, doi: 10.1109/TIE.2015. 2417122.

[77] G. Ke, Q. Chen, W. Gao, S.-C. Wong, C. K. Tse, and Z. Zhang, "Research on IPT resonant converters with high misalignment tolerance using multicoil receiver set," *IEEE Trans. Power Electron.*, vol. 35, no. 4, pp. 3697–3712, Apr. 2020, doi: 10.1109/TPEL.2019.2936325.

[78] S. Song, Q. Zhang, Z. He, H. Li, and X. Zhang, "Uniform power dynamic wireless charging system with I-type power supply rail and DQ-phase-receiver employing receiver-side control," *IEEE Trans. Power Electron.*, vol. 35, no. 10, pp. 11205–11212, Oct. 2020, doi: 10.1109/TPEL.2020.2979029.

[79] Q. Zhang, S. Song, S. Dong, and C. Zhu, "Receiver-side-oriented simulator for dynamic wireless charging system with I-type transmitter and multiphase receiver," *IEEE Trans. Ind. Electron.*, vol. 68, no. 5, pp. 3906–3916, May 2021, doi: 10.1109/TIE.2020.2982087.

[80] A. Kamineni, G. A. Covic, and J. T. Boys, "Analysis of coplanar intermediate coil structures in inductive power transfer systems," *IEEE Trans. Power Electron.*, vol. 30, no. 11, pp. 6141–6154, Nov. 2015, doi: 10.1109/TPEL.2014.2378733.

[81] S. Moon, B.-C. Kim, S.-Y. Cho, C.-H. Ahn, and G.-W. Moon, "Analysis and design of a wireless power transfer system with an intermediate coil for high efficiency," *IEEE Trans. Ind. Electron.*, vol. 61, no. 11, pp. 5861–5870, Nov. 2014, doi: 10.1109/TIE.2014.2301762.

[82] S. Moon and G.-W. Moon, "Wireless power transfer system with an asymmetric four-coil resonator for electric vehicle battery chargers," *IEEE Trans. Power Electron.*, vol. 31, no. 10, pp. 6844–6854, Oct. 2016, doi: 10.1109/TPEL.2015.2506779.

[83] D. H. Tran, V. B. Vu, and W. Choi, "Design of a high-efficiency wireless power transfer system with intermediate coils for the on-board chargers of electric vehicles," *IEEE Trans. Power Electron.*, vol. 33, no. 1, pp. 175–187, Jan. 2018, doi: 10.1109/TPEL.2017.2662067.

[84] W. Li, H. Zhao, S. Li, J. Deng, T. Kan, and C. C. Mi, "Integrated *LCC* compensation topology for wireless charger in electric and plug-in electric vehicles," *IEEE Trans. Ind. Electron.*, vol. 62, no. 7, pp. 4215–4225, Dec. 2015, doi: 10.1109/TIE.2014.2384003.

[85] J. Deng, W. Li, T. D. Nguyen, S. Li, and C. C. Mi, "Compact and efficient bipolar coupler for wireless power chargers: Design and analysis," *IEEE Trans. Power Electron.*, vol. 30, no. 11, pp. 6130–6140, Nov. 2015, doi: 10.1109/TPEL.2015.2417115.

[86] T. Kan, T.-D. Nguyen, J. C. White, R. K. Malhan, and C. C. Mi, "A new integration method for an electric vehicle wireless charging system using LCC compensation topology: Analysis and design," *IEEE Trans. Power Electron.*, vol. 32, no. 2, pp. 1638–1650, Feb. 2017, doi: 10.1109/TPEL.2016.2552060.

[87] T. Kan, F. Lu, T.-D. Nguyen, P. P. Mercier, and C. C. Mi, "Integrated coil design for EV wireless charging systems using LCC compensation topology," *IEEE Trans. Power Electron.*, vol. 33, no. 11, pp. 9231–9241, Nov. 2018, doi: 10.1109/TPEL.2018.2794448.

[88] A. Ramezani and M. Narimani, "A new wireless EV charging system with integrated DC–DC magnetic element," *IEEE Trans. Transport. Electrific.*, vol. 5, no. 4, pp. 1112–1123, Dec. 2019, doi: 10.1109/TTE.2019.2955251.

[89] A. Ramezani and M. Narimani, "Optimal design of fully integrated magnetic structure for wireless charging of electric vehicles," *IEEE Trans. Transport. Electrific.*, vol. 7, no. 4, pp. 2114–2127, Dec. 2021, doi: 10.1109/TTE.2021.3067875.

[90] V.-B. Vu, J. M. Gonzalez-Gonzalez, V. Pickert, M. Dahidah, and A. Trivino, "A hybrid charger of conductive and inductive modes for electric vehicles," *IEEE Trans. Ind. Electron.*, vol. 68, no. 12, pp. 12021–12033, Dec. 2021, doi: 10.1109/TIE.2020.3042162.

[91] A. A. S. Mohamed and O. A. Mohammed, "Integrated bidirectional inductive/conductive electrical apparatus," U.S. Patent 15/848445, Jun. 20, 2019.

[92] W. Liu, K. T. Chau, C. H. T. Lee, W. Han, X. Tian, and W. H. Lam, "Full-range soft-switching pulse frequency modulated wireless power transfer," *IEEE Trans. Power Electron.*, vol. 35, no. 6, pp. 6533–6547, Jun. 2020, doi: 10.1109/TPEL.2019.2952573.

[93] S.-J. Huang, T.-S. Lee, W.-H. Li, and R.-Y. Chen, "Modular on-road AGV wireless charging systems via interoperable power adjustment," *IEEE Trans. Ind. Electron.*, vol. 66, no. 8, pp. 5918–5928, Aug. 2019, doi: 10.1109/TIE.2018.2873165.

[94] P. S. Huynh and S. S. Williamson, "Analysis and design of soft-switching active-clamping half-bridge boost inverter for inductive wireless charging applications," *IEEE Trans. Transport. Electrific.*, vol. 5, no. 4, pp. 1027–1039, Dec. 2019, doi: 10.1109/TTE.2019.2930199.

[95] A. Namadmalan, "Self-oscillating pulsewidth modulation for inductive power transfer systems," *IEEE J. Emerg. Sel. Topics Power Electron.*, vol. 8, no. 2, pp. 1813–1820, Jun. 2020, doi: 10.1109/ JESTPE.2019.2916425.

[96] R. Mai, Z. Yan, Y. Chen, S. Liu, and Z. He, "A hybrid transmitter-based efficiency improvement controller with full-bridge dual resonant tank for misalignment condition," *IEEE Trans. Power Electron.*, vol. 35, no. 1, pp. 1124–1135, Jan. 2020, doi: 10.1109/TPEL.2019.2916231.

[97] J. L. Villa, J. Sallan, J. F. S. Osorio, and A. Llombart, "High-misalignment tolerant compensation topology for ICPT systems," *IEEE Trans. Ind. Electron.*, vol. 59, no. 2, pp. 945–951, Feb. 2012, doi: 10.1109/TIE.2011.2161055.

[98] Y. Wang, Y. Yao, X. Liu, and D. Xu, "S/CLC compensation topology analysis and circular coil design for wireless power transfer," *IEEE Trans. Transport. Electrific.*, vol. 3, no. 2, pp. 496–507, Jun. 2017, doi: 10.1109/TTE.2017.2651067.

[99] W. Li, H. Zhao, J. Deng, S. Li, and C. C. Mi, "Comparison study on SS and double-sided LCC compensation topologies for EV/PHEV wireless chargers," *IEEE Trans. Veh. Technol.*, vol. 65, no. 6, pp. 4429–4439, Jun. 2016, doi: 10.1109/TVT.2015.2479938.

[100] B. Wang, A. P. Hu, and D. Budgett, "Maintaining middle zero voltage switching operation of parallel–parallel tuned wireless power transfer system under bifurcation," *IET Power Electron.*, vol. 7, no. 1, pp. 78–84, Jan. 2014, doi: 10.1049/IET-PEL.2013.0250.

[101] H. Feng, T. Cai, S. Duan, J. Zhao, X. Zhang, and C. Chen, "An LCC-compensated resonant converter optimized for robust reaction to large coupling variation in dynamic wireless power transfer," *IEEE Trans. Ind. Electron.*, vol. 63, no. 10, pp. 6591–6601, Oct. 2016, doi: 10.1109/TIE.2016.2589922.

[102] M. Borage, S. Tiwari, and S. Kotaiah, "Analysis and design of an LCL-T resonant converter as a constant-current power supply," *IEEE Trans. Ind. Electron.*, vol. 52, no. 6, pp. 1547–1554, Dec. 2005, doi: 10.1109/TIE.2005.858729.

[103] C.-S. Wang, G. A. Covic, and O. H. Stielau, "Investigating an LCL load resonant inverter for inductive power transfer applications," *IEEE Trans. Power Electron.*, vol. 19, no. 4, pp. 995–1002, Jul. 2004, doi: 10.1109/TPEL.2004.830098.

[104] B. Esteban, M. Sid-Ahmed, and N. C. Kar, "A comparative study of power supply architectures in wireless EV charging systems," *IEEE Trans. Power Electron.*, vol. 30, no. 11, pp. 6408–6422, Nov. 2015, doi: 10.1109/TPEL.2015.2440256.

[105] D. Shen, G. Du, W. Zeng, Z. Yang, and J. Li, "Research on optimization of compensation topology parameters for a wireless power transmission system with wide coupling coefficient fluctuation," *IEEE Access*, vol. 8, pp. 59648–59658, 2020, doi: 10.1109/ACCESS.2020. 2983612.

[106] J. Zhang *et al.*, "Total harmonic distortion and output current optimization method of inductive power transfer system for power loss reduction," *IEEE Access*, vol. 8, pp. 4724–4736, 2020, doi: 10.1109/ ACCESS.2019.2962900.

[107] S. Chen *et al.*, "An operation mode selection method of dual-side bridge converters for efficiency optimization in inductive power transfer," *IEEE Trans. Power Electron.*, vol. 35, no. 10, pp. 9992–9997, Oct. 2020, doi: 10.1109/TPEL.2020.2979769.

[108] Y. Li *et al.*, "Efficiency analysis and optimization control for input-parallel output-series wireless power transfer systems," *IEEE Trans. Power Electron.*, vol. 35, no. 1, pp. 1074–1085, Jan. 2020, doi: 10.1109/TPEL.2019.2914299.

[109] L. Yang, X. Li, S. Liu, Z. Xu, and C. Cai, "Analysis and design of an LCCC/S-compensated WPT system with constant output characteristics for battery charging applications," *IEEE J. Emerg. Sel. Topics Power Electron.*, vol. 9, no. 1, pp. 1169–1180, Feb. 2021, doi: 10.1109/JESTPE.2020.2971583.

[110] H. H. Wu, A. Gilchrist, K. D. Sealy, and D. Bronson, "A high efficiency 5 kW inductive charger for EVs using dual side control," *IEEE Trans. Ind. Informat.*, vol. 8, no. 3, pp. 585–595, Aug. 2012, doi: 10.1109/TII.2012.2192283.

[111] J. Lu, G. Zhu, H. Wang, F. Lu, J. Jiang, and C. C. Mi, "Sensitivity analysis of inductive power transfer systems with voltage-fed compensation topologies," *IEEE Trans. Veh. Technol.*, vol. 68, no. 5, pp. 4502–4513, May 2019, doi: 10.1109/TVT.2019.2903565.

[112] B.-V. Vu, V.-T. Phan, M. Dahidah, and V. Pickert, "Multiple output inductive charger for electric vehicles," *IEEE Trans. Power Electron.*, vol. 34, no. 8, pp. 7350–7368, Aug. 2019, doi: 10.1109/TPEL.2018.2882945.

[113] Y. Chen, H. Zhang, C.-S. Shin, C.-H. Jo, S.-J. Park, and D.-H. Kim, "An efficiency optimization-based asymmetric tuning method of double-sided LCC compensated WPT system for electric vehicles," *IEEE Trans. Power Electron.*, vol. 35, no. 11, pp. 11475–11487, Nov. 2020, doi: 10.1109/TPEL.2020.2984712.

[114] X. Zhang, Y. Zhang, Z. Zhang, and M. Li, "Mode conversion and structure optimization of quadrature coils for electric vehicles wireless power transfer," *IEEE Trans. Energy Convers.*, vol. 35, no. 2, pp. 575–590, Jun. 2020, doi: 10.1109/TEC.2020.2972584.

[115] G. Yang *et al.*, "Interoperability improvement for wireless electric vehicle charging system using adaptive phase-control transmitter," *IEEE Access*, vol. 7, pp. 41365–41379, 2019, doi: 10.1109/ACCESS.2019.2907741.

[116] Y. Guo, L. Wang, Y. Zhang, S. Li, and C. Liao, "Rectifier load analysis for electric vehicle wireless charging system," *IEEE Trans. Ind. Electron.*, vol. 65, no. 9, pp. 6970–6982, Sep. 2018, doi: 10.1109/TIE.2018.2793260.

[117] V.-B. Vu, D.-H. Tran, and W. Choi, "Implementation of the constant current and constant voltage charge of inductive power transfer systems with the double-sided LCC compensation topology for electric vehicle battery charge applications," *IEEE Trans. Power Electron.*, vol. 33, no. 9, pp. 7398–7410, Sep. 2018, doi: 10.1109/TPEL.2017.2766605.

[118] F. Lu, H. Zhang, H. Hofmann, W. Su, and C. C. Mi, "A dual-coupled LCC-compensated IPT system with a compact magnetic coupler," *IEEE Trans. Power Electron.*, vol. 33, no. 7, pp. 6391–6402, Jul. 2018, doi: 10.1109/TPEL.2017.2748391.

[119] N. Keeling, G. A. Covic, F. Hao, L. George, and J. T. Boys, "Variable tuning in LCL compensated contactless power transfer pickups," in *Proc. IEEE Energy Convers. Congr. Expo.*, Sep. 2009, pp. 1826–1832, doi: 10.1109/ECCE.2009.5316169.

[120] S. Aldhaher, P.-K. Luk, A. Bati, and J. Whidborne, "Wireless power transfer using class E inverter with saturable DC-feed inductor," *IEEE Trans. Ind. Appl.*, vol. 50, no. 4, pp. 2710–2718, Jul. 2014, doi: 10.1109/TIA.2014.2300200.

[121] S. Aldhaher, P. C.-K. Luk, and J. F. Whidborne, "Electronic tuning of misaligned coils in wireless power transfer systems," *IEEE Trans. Power Electron.*, vol. 29, no. 11, pp. 5975–5982, Nov. 2014, doi: 10.1109/TPEL.2014.2297993.

[122] K. A. Cota, P. A. Gray, M. Pathmanathan, and P. W. Lehn, "An approach for selecting compensation capacitances in resonance-based EV wireless power transfer systems with switched capacitors," *IEEE Trans. Transport. Electrific.*, vol. 5, no. 4, pp. 1004–1014, Dec. 2019, doi: 10.1109/TTE.2019.2927803.

[123] J. Zhao, J. Zhang, and Y. Zhu, "A flexible wireless power transfer system with switch controlled capacitor," *IEEE Access*, vol. 7, pp. 106873–106881, 2019, doi: 10.1109/ACCESS.2019.2929516.

[124] D.-H. Kim and D. Ahn, "Self-tuning LCC inverter using PWM-controlled switched capacitor for inductive wireless power transfer," *IEEE Trans. Ind. Electron.*, vol. 66, no. 5, pp. 3983–3992, May 2019, doi: 10.1109/TIE.2018.2844796.

[125] J. Zhang, J. Zhao, Y. Zhang, and F. Deng, "A wireless power transfer system with dual switch-controlled capacitors for efficiency optimization," *IEEE Trans. Power Electron.*, vol. 35, no. 6, pp. 6091–6101, Jun. 2020, doi: 10.1109/TPEL.2019.2950218.

[126] L. Zhao, D. Thrimawithana, and U. K. Madawala, "Hybrid bidirectional wireless EV charging system tolerant to pad misalignment," *IEEE Trans. Ind. Electron.*, vol. 64, no. 9, pp. 7079–7086, Sep. 2017, doi: 10.1109/TIE.2017.2686301.

[127] R. Mai, Y. Chen, Y. Li, Y. Zhang, G. Cao, and Z. He, "Inductive power transfer for massive electric bicycles charging based on hybrid topology switching with a single inverter," *IEEE Trans. Power Electron.*, vol. 32, no. 8, pp. 5897–5906, Aug. 2017, doi: 10.1109/TPEL.2017.2654360.

[128] Y. Li, Q. Xu, T. Lin, J. Hu, Z. He, and R. Mai, "Analysis and design of load-independent output current or output voltage of a three-coil wireless power transfer system," *IEEE Trans. Transport. Electrific.*, vol. 4, no. 2, pp. 364–375, Jun. 2018, doi: 10.1109/TTE.2018.2808698.

[129] Y. Li, J. Hu, F. Chen, S. Liu, Y. Zhaotian, and Z. He, "A new-variable-coil-structure-based IPT system with load-independent constant output current or voltage for charging electric bicycles," *IEEE Trans. Power Electron.*, vol. 33, no. 10, pp. 8226–8230, Oct. 2018, doi: 10.1109/TPEL.2018.2812716.

[130] Y. Chen, B. Yang, Z. Kou, Z. He, G. Cao, and R. Mai, "Hybrid and reconfigurable IPT systems with high-misalignment tolerance for constant-current and constant-voltage battery charging," *IEEE Trans. Power Electron.*, vol. 33, no. 10, pp. 8259–8269, Oct. 2018, doi: 10.1109/TPEL.2018.2809785.

[131] H. Feng, T. Cai, S. Duan, X. Zhang, H. Hu, and J. Niu, "A dual-side-detuned series–series compensated resonant converter for wide charging region in a wireless power transfer system," *IEEE Trans. Ind. Electron.*, vol. 65, no. 3, pp. 2177–2188, Mar. 2018, doi: 10.1109/TIE.2017.2745455.

[132] A. Hakemi, D. Jovanovic, D. M. Vilathgamuwa, G. Walker, and J. Pauls, "Generic uncertainty parameter analysis and optimization of series–series wireless power transfer system for robust controller design," *IEEE Trans. Ind. Electron.*, vol. 69, no. 4, pp. 4107–4118, Apr. 2022, doi: 10.1109/TIE.2021.3071689.

[133] J. Zhao, T. Cai, S. Duan, H. Feng, C. Chen, and X. Zhang, "A general design method of primary compensation network for dynamic WPT system maintaining stable transmission power," *IEEE Trans. Power Electron.*, vol. 31, no. 12, pp. 8343–8358, Dec. 2016, doi: 10.1109/TPEL.2016.2516023.

[134] Q. Zhu, Y. Guo, L. Wang, C. Liao, and F. Li, "Improving the misalignment tolerance of wireless charging system by optimizing the compensate capacitor," *IEEE Trans. Ind. Electron.*, vol. 62, no. 8, pp. 4832–4836, Aug. 2015, doi: 10.1109/TIE.2015.2397882.

[135] Y. Yao, Y. Wang, X. Liu, Y. Pei, D. G. Xu, and X. Liu, "Particle swarm optimization-based parameter design method for S/CLC-compensated IPT systems featuring high tolerance to misalignment and load variation," *IEEE Trans. Power Electron.*, vol. 34, no. 6, pp. 5268–5282, Jun. 2019, doi: 10.1109/TPEL.2018.2870530.

[136] Y. Wang, J. Mai, Y. Yao, and D. Xu, "Analysis and design of an IPT system based on S/SP compensation with improved output voltage regulation," *IEEE Trans. Ind. Informat.*, vol. 16, no. 5, pp. 3256–3266, May 2020, doi: 10.1109/TII.2019.2952918.

[137] Y. Yao, Y. Wang, X. Liu, K. Lu, and D. Xu, "Analysis and design of an S/SP compensated IPT system to minimize output voltage fluctuation versus coupling coefficient and load variation," *IEEE Trans. Veh. Technol.*, vol. 67, no. 10, pp. 9262–9272, Oct. 2018, doi: 10.1109/TVT.2018.2855682.

[138] W. Bronzi, T. Derrmann, G. Castignani, and T. Engel, "Towards characterizing Bluetooth discovery in a vehicular context," in *Proc. IEEE Veh. Netw. Conf. (VNC)*, Dec. 2016, pp. 1–4, doi: 10.1109/VNC.2016.7835935.

[139] J. M. Gonzalez-Gonzalez, A. Trivino-Cabrera, and J. A. Aguado, "Model predictive control to maximize the efficiency in EV wireless chargers," *IEEE Trans. Ind. Electron.*, vol. 69, no. 2, pp. 1244–1253, Feb. 2022, doi: 10.1109/TIE.2021.3057006.

[140] A. A. S. Mohamed and O. Mohammed, "Bilayer predictive power flow controller for bidirectional operation of wirelessly connected electric vehicles," *IEEE Trans. Ind. Appl.*, vol. 55, no. 4, pp. 4258–4267, Jul. 2019, doi: 10.1109/TIA.2019.2908347.

[141] D. Yang, S. Won, J. Tian, Z. Cheng, and J. Kim, "A method of estimating mutual inductance and load resistance using harmonic components in wireless power transfer system," *Energies*, vol. 12, no. 14, p. 2728, Jul. 2019, doi: 10.3390/en12142728.

[142] V. Jiwariyavej, T. Imura, and Y. Hori, "Coupling coefficients estimation of wireless power transfer system via magnetic resonance coupling using information from either side of the system," *IEEE Trans. Emerg. Sel. Topics Power Electron.*, vol. 3, no. 1, pp. 191–200, Mar. 2015, doi: 10.1109/JESTPE.2014.2332056.

[143] W. Shi, J. Deng, Z. Wang, and X. Cheng, "The start-up dynamic analysis and one cycle control-PD control combined strategy for primary-side controlled wireless power transfer system," *IEEE Access*, vol. 6, pp. 14439–14450, 2018, doi: 10.1109/ACCESS.2018.2811179.

[144] C. Chen, H. Zhou, Q. Deng, W. Hu, Y. Yu, X. Lu, and J. Lai, "Modeling and decoupled control of inductive power transfer to implement constant current/voltage charging and ZVS operating for electric vehicles," *IEEE Access*, vol. 6, pp. 59917–59928, 2018, doi: 10.1109/ACCESS.2018.2875413.

[145] S. A. Sis and H. Akca, "Maximizing the efficiency of wireless power transfer systems with an optimal duty cycle operation," *AEU Int. J. Electron. Commun.*, vol. 116, Mar. 2020, Art. no. 153081, doi: 10.1016/j.aeue.2020.153081.

[146] J. González-González, A. Triviño-Cabrera, and J. Aguado, "Design and validation of a control algorithm for a SAE J2954-compliant wireless charger to guarantee the operational electrical constraints," *Energies*, vol. 11, no. 3, p. 604, Mar. 2018, doi: 10.3390/en11030604.

[147] P. K. Joseph, D. Elangovan, and G. Arunkumar, "Linear control of wireless charging for electric bicycles," *Appl. Energy*, vol. 255, Dec. 2019, Art. no. 113898, doi: 10.1016/j.apenergy.2019.113898.

[148] N.-C. Kuo, B. Zhao, and A. M. Niknejad, "Bifurcation analysis in weakly-coupled inductive power transfer systems," *IEEE Trans. Circuits Syst. I, Reg. Papers*, vol. 63, no. 5, pp. 727–738, May 2016, doi: 10.1109/TCSI.2016.2529283.

[149] E. Gati, G. Kampitsis, and S. Manias, "Variable frequency controller for inductive power transfer in dynamic conditions," *IEEE Trans. Power Electron.*, vol. 32, no. 2, pp. 1684–1696, Feb. 2017, doi: 10.1109/TPEL.2016.2555963.

[150] J. M. Miller, O. C. Onar, and M. Chinthavali, "Primary-side power flow control of wireless power transfer for electric vehicle charging," *IEEE J. Emerg. Sel. Topics Power Electron.*, vol. 3, no. 1, pp. 147–162, Mar. 2015, doi: 10.1109/JESTPE.2014.2382569.

[151] Y. Jiang, L. Wang, Y. Wang, J. Liu, X. Li, and G. Ning, "Analysis, design, and implementation of accurate ZVS angle control for EV battery charging in wireless high-power transfer," *IEEE Trans. Ind. Electron.*, vol. 66, no. 5, pp. 4075–4085, May 2019, doi: 10.1109/TIE.2018.2795523.

[152] Y. Chen, Z. Kou, Y. Zhang, Z. He, R. Mai, and G. Cao, "Hybrid topology with configurable charge current and charge voltage output-based WPT charger for massive electric bicycles," *IEEE J. Emerg. Sel. Topics Power Electron.*, vol. 6, no. 3, pp. 1581–1594, Sep. 2018, doi: 10.1109/JESTPE.2017.2782269.

[153] D. Kobayashi, T. Imura, and Y. Hori, "Real-time coupling coefficient estimation and maximum efficiency control on dynamic wireless power transfer for electric vehicles," in *Proc. IEEE PELS Workshop Emerg. Technol., Wireless Power (WoW)*, Jun. 2015, pp. 1–6, doi: 10.1109/WoW.2015.7132799.

[154] C. Chen, G. A. Covic, and J. T. Boys, "Regulator capacitor selection for series compensated IPT pickups," in *Proc. 34th Annu. Conf. IEEE Ind. Electron.*, Nov. 2008, pp. 932–937, doi: 10.1109/IECON.2008.4758078.

[155] N. A. Keeling, G. A. Covic, and J. T. Boys, "A unity-power-factor IPT pickup for high-power applications," *IEEE Trans. Ind. Electron.*, vol. 57, no. 2, pp. 744–751, Feb. 2010, doi: 10.1109/TIE.2009.2027255.

[156] A. Kouzou, "Power factor correction circuits," in *Power Electronics Handbook*, 4th ed., M. H. Rashid, Ed. Oxford, U.K.: Butterworth-Heinemann, 2016, pp. 529–569, doi: 10.1016/B978-0-12-811407-0.00017-9.

[157] X. Dai, X. Li, Y. Li, P. Deng, and C. Tang, "A maximum power transfer tracking method for WPT systems with coupling coefficient identification considering two-value problem," *Energies*, vol. 10, no. 10, p. 1665, Oct. 2017, doi: 10.3390/en10101665.

[158] J. Kikuchi, M. D. Manjrekar, and T. A. Lipo, "Performance improvement of half controlled three phase PWM boost rectifier," in *Proc. 30th Annu. IEEE Power Electron. Spec. Conf. Record.*, Jul. 1999, pp. 319–324, doi: 10.1109/PESC.1999.789022.

[159] B.-R. Lin and Z.-L. Hung, "A single-phase bidirectional rectifier with power factor correction," in *Proc. IEEE Region 10 Int. Conf. Electr. Electron. Technol. (TENCON)*, Aug. 2001, pp. 601–605, doi: 10.1109/TENCON.2001.949665.

[160] K. Colak, E. Asa, M. Bojarski, D. Czarkowski, and O. C. Onar, "A novel phase-shift control of semibridgeless active rectifier for wireless power transfer," *IEEE Trans. Power Electron.*, vol. 30, no. 11, pp. 6288–6297, Nov. 2015, doi: 10.1109/TPEL.2015.2430832.

[161] J. H. Lee, W.-J. Son, S. Ann, J. Byun, and B. K. Lee, "Improved pulse density modulation with a distribution algorithm for semi-bridgeless rectifier of inductive power transfer system in electric vehicles," in *Proc. 10th Int. Conf. Power Electron. ECCE Asia (ICPE-ECCE Asia)*, May 2019, pp. 1–6, doi: 10.23919/ICPE2019-ECCEAsia42246.2019.8797336.

[162] M. Fan, L. Shi, Z. Yin, and Y. Li, "A novel pulse density modulation with semi-bridgeless active rectifier in inductive power transfer system for rail vehicle," *CES Trans. Electr. Mach. Syst.*, vol. 1, no. 4, pp. 397–404, Dec. 2017, doi: 10.23919/TEMS.2017.8241361.

[163] T. Diekhans and R. W. D. Doncker, "A dual-side controlled inductive power transfer system optimized for large coupling factor variations and partial load," *IEEE Trans. Power Electron.*, vol. 30, no. 11, pp. 6320–6328, Nov. 2015, doi: 10.1109/TPEL.2015.2393912.

[164] W. Zhong and S. Y. R. Hui, "Charging time control of wireless power transfer systems without using mutual coupling information and wireless communication system," *IEEE Trans. Ind. Electron.*, vol. 64, no. 1, pp. 228–235, Jan. 2017, doi: 10.1109/TIE.2016.2598725.

[165] H. Li, J. Li, K. Wang, W. Chen, and X. Yang, "A maximum efficiency point tracking control scheme for wireless power transfer systems using magnetic resonant coupling," *IEEE Trans. Power Electron.*, vol. 30, no. 7, pp. 3998–4008, Jul. 2015, doi: 10.1109/TPEL.2014.2349534.

[166] W. X. Zhong and S. Y. R. Hui, "Maximum energy efficiency tracking for wireless power transfer systems," *IEEE Trans. Power Electron.*, vol. 30, no. 7, pp. 4025–4034, Jul. 2015, doi: 10.1109/TPEL.2014.2351496.

[167] X. Dai, X. Li, Y. Li, and A. P. Hu, "Maximum efficiency tracking for wireless power transfer systems with dynamic coupling coefficient estimation," *IEEE Trans. Power Electron.*, vol. 33, no. 6, pp. 5005–5015, Jun. 2018, doi: 10.1109/TPEL.2017.2729083.

[168] H. Li, K. Wang, J. Fang, and Y. Tang, "Pulse density modulated ZVS full-bridge converters for wireless power transfer systems," *IEEE Trans. Power Electron.*, vol. 34, no. 1, pp. 369–377, Jan. 2019, doi: 10.1109/TPEL.2018.2812213.

[169] Y. Narusue, Y. Kawahara, and T. Asami, "Maximum efficiency point tracking by input control for a wireless power transfer system with a switching voltage regulator," in *Proc. IEEE Wireless Power Transf. Conf. (WPTC)*, May 2015, pp. 1–4, doi: 10.1109/WPT.2015.7140139.

[170] M. Wu et al., "A dual-sided control strategy based on mode switching for efficiency optimization in wireless power transfer system," *IEEE Trans. Power Electron.*, vol. 36, no. 8, pp. 8835–8848, Aug. 2021, doi: 10.1109/TPEL.2021.3055963.

[171] L. Hutchinson, B. Waterson, B. Anvari, and D. Naberezhnykh, "Potential of wireless power transfer for dynamic charging of electric vehicles," *IET Intell. Transp. Syst.*, vol. 13, no. 1, pp. 3–12, Jul. 2018, doi: 10.1049/iet-its.2018.5221.

[172] K. Hwang et al., "An autonomous coil alignment system for the dynamic wireless charging of electric vehicles to minimize lateral misalignment," *Energies*, vol. 10, no. 3, p. 315, Mar. 2017, doi: 10.3390/en10030315.

Van-Binh Vu (Member, IEEE) received the bachelor's degree (Talented Program) from the Hanoi University of Science and Technology, Hanoi, Vietnam, in 2014, the master's degree from Soongsil University, Seoul, Republic of Korea, in 2016, and the Ph.D. degree from Newcastle University, Newcastle upon Tyne, U.K., in 2020, all in electrical engineering.

He is currently with Turbo Power Systems, Gateshead, U.K., responsible for the development of grid-connected converters. He also holds a research position at the Electrical Power Group, Newcastle University. He has published in the top-tier IEEE journals in power electronics. His main research area includes the fields of power electronics, especially wireless power transfer for electric vehicles.

Dr. Vu has served as a regular reviewer for both IEEE and IET journals.

Ali Ramezani (Member, IEEE) received the B.Sc. degree in electrical engineering from Shahid Beheshti University, Tehran, Iran, in 2014, the M.Sc. degree in electrical engineering from the University of Tehran, Tehran, in 2017, and the Ph.D. degree from the Department of Electrical and Computer Engineering, McMaster University, Hamilton, ON, Canada, in 2021.

He is currently an Electrical Engineer with eLeap-Power, Toronto, ON, Canada. His research interests include wireless power transfer, design and control of the automotive high-power converters, magnetic design, and renewable energy sources.

Alicia Triviño (Member, IEEE) was born in Málaga, Spain. She received the bachelor's degree in telecommunication and the Ph.D. degree in computer science from the University of Málaga, Málaga, in 2002 and 2008, respectively.

She is currently an Associate Professor with the University of Málaga. Her research interests include wireless power transfer and electric vehicles wireless chargers. She has actively participated in the design and development of three prototypes including features as bidirectionality and dynamic charge.

José M. González-González was born in Málaga, Spain. He received the M.Sc. degree in industrial engineering from the University of Málaga, Málaga, in 2015, where he is currently pursuing the Ph.D. degree in wireless power transfer in electric vehicles with a focus on the design of a prototype with bidirectional features.

He has authored on topics related to the integration of battery energy storage.

Nasiru B. Kadandani (Member, IEEE) received the B.Eng. and M.Eng. degrees in electrical engineering from Bayero University Kano, Kano, Nigeria, in 2004 and 2010, respectively, and the Ph.D. degree in electrical engineering from Newcastle University, Newcastle upon Tyne, U.K., in 2021.

He is currently with the Electrical Power Research Group, School of Engineering, Newcastle University. He has authored or coauthored over 30 research articles published in referenced journals and conference proceedings. His current research interests include multilevel converters, solid-state transformers, wind energy conversion systems, grid integration of renewable energy, and electric vehicle charging systems.

Dr. Kadandani is also a Registered Member of the Council for the Regulation of Engineering in Nigeria (COREN) and the Nigerian Society of Engineers (NSE). He was the Nigerian representative during the 9th International Training on Wind Turbine Technology and Applications held at the National Institute of Wind Energy (NIWE), formerly Centre for Wind Energy Technology (C-WET), Chennai, India, in 2012.

Mohamed Dahidah (Senior Member, IEEE) received the Ph.D. degree in electrical engineering from Multimedia University, Cyberjaya, Malaysia, in 2008.

He was an Assistant Professor with the Department of Electrical and Electronic Engineering, The University of Nottingham, Malaysia Campus, Semenyih, Malaysia, until November 2012. He is currently a Senior Lecturer with the School of Engineering, Newcastle University, Newcastle Upon Tyne, U.K. He has authored or coauthored over 80 refereed journal articles and conference papers in the field of power electronics. His current research interests include modular power converters, battery chargers for electric vehicles (EVs), solid-state transformers, and advanced power conversion for renewable energy integration.

Dr. Dahidah was a recipient of the Frist Prize Paper Award at IEEE Conference on Sustainable Utilization and Development in Engineering and Technology, Kuala Lumpur, Malaysia, in 2010, and the Girling Watson Fellowship Award at The University of Sydney, Australia, in 2009. He is also the Deputy Editor-in-Chief of *IET Power Electronics*. He has been a regular reviewer for both IEEE and IET journals.

Volker Pickert (Member, IEEE) studied at RWTH Aachen University, Aachen, Germany, and Cambridge University, Cambridge, U.K. He received the Dipl.Ing. degree in electrical and electronic engineering from RWTH Aachen University in 1994 and the Ph.D. degree in power electronics from Newcastle University, Newcastle upon Tyne, U.K., in 1997.

From 1998 to 1999, he was an Application Engineer with Semikron GmbH, Nuremberg, Germany. From 1999 to 2003, he was a Group Leader with Volkswagen AG, Wolfsburg, Germany, responsible for the development of electric drives for electric vehicles. In 2003, he was appointed as a Senior Lecturer at the Electrical Power Group, Newcastle University, where he became a Full Professor of power electronics in 2011. In 2012, he became the Head of the Electrical Power Group and, in 2020, the Director of Discipline for Electrical and Electronic Engineering at Newcastle University. He has published more than 180 book chapters, journal articles, and conference papers in the area of power electronics and electric drives. His current research interests include power electronics for transport applications, thermal management, health monitoring techniques, and advanced nonlinear control.

Prof. Pickert received the IMarEST Denny Medal for the best article in the *Journal of Marine Engineering* in 2011. In 2018, he received the Best Paper Award at IEEE International Conference on Computing Electronics & Communications Engineering (iCCECE), Essex, U.K. He is regularly invited as a keynote speaker and advises various governments on energy and transport-related issues. In 2019, he became the Director of U.K.'s EPSRC Doctoral Training Centre in Power Electronics for Sustainable Electric Propulsion. He is also the active Editor-in-Chief of the *IET Power Electronics* journal.

Mehdi Narimani (Senior Member, IEEE) received the Ph.D. degree in electrical engineering from the University of Western Ontario, London, ON, Canada, in 2012.

He was a Power Electronics Engineer with Rockwell Automation Canada, Cambridge, ON, Canada. He is currently an Associate Professor with the Department of Electrical and Computer Engineering, McMaster University, Hamilton, ON, Canada. He has authored/coauthored more than 140 journal articles and conference proceeding papers, coauthored a Wiley-IEEE Press book, and holds seven issued/pending U.S./European patents. His current research interests include power conversion, high-power converters, control of power electronics converters, fast electric vehicle (EV) chargers, and wireless EV charging systems.

Dr. Narimani also holds the NSERC Canada Research Chair (CRC) position in high-power converter systems.

Jose Aguado (Member, IEEE) was born in Málaga, Spain. He received the Electrical Engineer and Ph.D. degrees from the University of Málaga, Málaga, in 1997 and 2001, respectively.

He is currently a Full Professor and the Head of the Electrical Engineering Department, University of Málaga. He has led more than 40 publicly funded research and consulting projects on the operation and planning of smart grids and wireless power transfer.